Simulating the Early Holocene demise of the Laurentide Ice Sheet with BISICLES (public trunk revision 3298)

Ilkka S.O. Matero[1,2], Lauren J. Gregoire[1], and Ruza F. Ivanovic[1]

[1]University of Leeds, United Kingdom
[2]Alfred Wegener Institute, Germany

Correspondence: Ilkka Matero (ilkka.matero@awi.de)

Abstract. Simulating the demise of the Laurentide Ice Sheet covering the Hudson Bay in the early Holocene (10-7 ka) is important for understanding the role of accelerated changes in ice sheet topography and melt in the '8.2 ka event', a century long cooling of the Northern Hemisphere by several degrees. Freshwater released from the ice sheet through a surface mass balance instability (known as the *saddle collapse*) has been suggested as a major forcing for the 8.2 ka event, but the temporal

5   evolution of this pulse has not been constrained. Dynamical ice loss and marine interactions could have significantly accelerated the ice sheet demise, but simulating such processes requires computationally expensive models that are difficult to configure and are often impractical for simulating past ice sheets. Here, we developed an ice sheet model setup for studying the Laurentide Ice Sheet's Hudson Bay saddle collapse and the associated meltwater pulse in unprecedented detail using the BISICLES ice sheet model, an efficient marine ice sheet model of the latest generation, capable of refinement to kilometre-scale resolution

10   and higher-order ice flow physics. The setup draws on previous efforts to model the deglaciation of the North American Ice Sheet for initialising the ice sheet temperature, recent ice sheet reconstructions for developing the topography of the region and ice sheet, and output from a general circulation model for a representation of the climatic forcing. The modelled deglaciation is in agreement with the reconstructed extent of the ice sheet and the associated meltwater pulse has realistic timing. Furthermore, the peak magnitude of the modelled meltwater equivalent (0.07-0.13 Sv) is compatible with geological estimates of freshwater

15   discharge through the Hudson Strait. The results demonstrate that while improved representation of the glacial dynamics and marine interactions are key for correctly simulating the pattern of early Holocene ice sheet retreat, surface mass balance introduces by far the most uncertainty. The new model configuration presented here provides future opportunities to quantify the range of plausible amplitudes and durations of a Hudson Bay ice saddle collapse meltwater pulse and its role in forcing the 8.2 ka event.

1 Introduction

A centennial-scale meltwater pulse produced by the collapse of an Ice Sheet that once covered Hudson Bay has been shown to be the possible driver of the most pronounced climatic perturbation of the Holocene, the 8.2 ka event (Matero et al., 2017), supported by recent geochemical evidence (Lochte et al., 2019). This so-called Hudson Bay Saddle Collapse resulted from an

5 acceleration in melting as the region connecting the Keewatin and Labrador ice domes became subject to increasingly negative surface mass balance (SMB) through a positive feedback with surface lowering (Gregoire et al., 2012). Gregoire et al. (2012) simulated an acceleration of melt lasting about 800 years and peaking at 0.2 Sv, which produced a 2.5 m contribution to sea level rise in 200 years caused by the separation of three ice sheet domes around Hudson Bay. While the saddle collapse mechanism described in this study is robust, the detailed evolution of the ice sheet did fully match empirical reconstructions,

10 with the separation of the Labrador, Keewatin and Baffin domes not occurring in the order suggested by geological evidence (Dyke, 2004). This mismatch between model results and geological evidence could have impacted the duration and amplitude of the simulated meltwater pulse. In addition, the deglaciation of the ice saddle could have been further accelerated through dynamic ice sheet instabilities such as grounding line destabilisation, ice streaming and increased calving at the marine terminus (Bassis et al., 2017). Contemporary continental ice sheets with marine margins are highly sensitive to these localised features

15 and require up to kilometre resolution to resolve them properly (Durand et al., 2009; Cornford et al., 2016). High-resolution ice sheet modelling simulations of these processes have not been previously conducted for the early-Holocene Laurentide Ice Sheet (LIS), and as a result a detailed model representation of the LIS saddle collapse and the resulting meltwater pulse remain knowledge gaps to be filled.

It is important to constrain the evolution of the saddle collapse in order to better understand the major forcing of the 8.2 ka

20 event, as both the modelled regional climate responses and the ocean circulation are sensitive to the duration and magnitude of the meltwater pulse (Matero et al., 2017). Changes in topography may play a secondary role, for example by modifying atmospheric circulation and thereby influencing North Atlantic Gyre circulation, but in this instance they are likely to be a much weaker forcing for climate change than freshwater released by the melting ice (Gregoire et al., 2018). Accurately representing the dynamical processes at marine margins of ice sheets has previously been challenging for studies of deglaciation

25 of continental-scale ice sheets, which takes place over several millennia, due to the high computational cost of the models. Application of Adaptive Mesh Refinement (AMR) is a pragmatic approach towards solving this problem by operating at a fine resolution in the dynamical regions, while keeping a coarser resolution where the ice is quiescent. AMR has been applied for simulating contemporary Antarctic and Greenland ice sheets in high detail in studies with the BISICLES ice sheet model (Cornford et al., 2013, 2015; Favier et al., 2014; Lee et al., 2015; Nias et al., 2016), and through good fit with

30 observed deglaciation and migration of the grounding line, these studies have demonstrated the usefulness of the model. They showed that the movement of the grounding line, overall mass loss and evolution of fast-flowing ice streams are all sensitive to increasing the mesh resolution and features in bed geometry (Cornford et al., 2015; Lee et al., 2015). A recent study applied BISICLES in a palaeo setting, focussing on simulating part of the British and Irish ice sheet, and highlighted the importance of marine interactions and marine ice sheet instability during the last deglaciation of the British Isles (Gandy et al., 2018).

However, applications of the BISICLES ice sheet model to simulating past ice sheet evolution have so far been limited to small ice sheets and have used idealised climate forcings. The present study addresses this directly, applying the BISICLES ice sheet model to simulating the demise of the Laurentide Ice Sheet in the early Holocene in order to better understand its late history and provide a useful model for improving constraints on meltwater, surface energy balance and topographic forcing of climate
5   around this time.

Ice sheets experience mass fluctuations as a result of the interplay between snow accumulation, ablation at the surfaces of the ice sheet and dynamical ice loss through calving (Bauer and Ganopolski, 2017). Representing the modes of ice loss in palaeo settings is challenging due to a lack of observational data for constraining the SMB as well as ice flow. The evolution of a simulated palaeo ice sheet cannot be directly compared with observations of SMB or ice flow, but instead reconstructions of
10   the evolution LIS extent and the positions of ice streams provide end-member constraints with which to compare and evaluate the results of the simulations. Two of the most recent LIS reconstructions are the commonly used ICE-6G_c (VM5a) reconstruction (henceforth "ICE-6G_c" Peltier et al., 2015) and the North American component of the GLAC-1D reconstruction (Tarasov et al., 2012). The ICE-6G_c reconstruction is based on Glacial Isostatic Adjustment (GIA) modelling and constrained by GPS observations of vertical motion of the crust, ice margin chronologies (Dyke, 2004), sea level rise (SLR) data and
15   space-based gravimetric measurements (Peltier et al., 2015). The global GLAC-1D reconstruction is combined from multiple sources (described in Ivanovic et al., 2016), of which the North American component is based on a dynamical ice sheet model constrained with relative sea level data (Tarasov et al., 2012, and references therein) and ice sheet extent from Dyke (2004). The evolution of the extent of LIS over the early-Holocene has been reconstructed from the timing of when individual locations became ice-free with an estimated error of ~500–800 years (Dyke, 2004; Margold et al., 2018). In terms of ice volume, the
20   reconstructions estimate that in the early Holocene (10 ka), LIS held ~11–18 m (GLAC-1D) and ~12.5 m (ICE-6G_c) global mean sea level rise equivalent, having already lost more than 80% of its Last Glacial Maximum mass.

We built a configuration of the BISICLES ice sheet model (Cornford et al., 2013) to simulate the early-Holocene LIS deglaciation based on information from the reconstructed evolution of the Laurentide Ice Sheet (ICE-6G_c and GLAC-1D) and a previous experiment that encompassed the deglaciation (Gregoire et al., 2012). The model setup was developed with the
25   aim of improving knowledge of the Hudson Bay saddle collapse through simulating the deglaciation with an updated climate forcing, finer spatial resolution and a more sophisticated representation of dynamical ice flow (including ice streams) compared to previous modelling studies of the time period (Marshall et al., 2002; Tarasov et al., 2012; Gregoire et al., 2012). As part of the setup, a selection of key parameters are varied individually to assess their role in model performance. The key parameters affecting ice flow are basal traction and the internal temperature structure of the ice sheet, and the key parameters affecting
30   SMB are the Positive-Degree-Day (PDD) factors defining the amount of snow and ice melt in response to the climate forcing (the SMB is represented through a PDD scheme, Rutt et al., 2009). In addition to these parameters and the mesh resolution, the effect of scaling the precipitation field is also evaluated as part of the sensitivity study, because the palaeo precipitation field from a single general circulation model (GCM) can exhibit significant regional biases (Knutti et al., 2010; Braconnot et al., 2012).

Geoscientific
Model Development
Discussions

2   The BISICLES ice sheet model

BISICLES is a vertically integrated ice flow model based on the 'L1L2' dynamical scheme devised by Schoof and Hindmarsh (2010), described in detail by Cornford et al. (2013). It has 10 vertical layers, which increase in thickness from 2% of ice thickness near the base to 15% of ice thickness near the surface. Ice in the model is assumed to be in hydrostatic equilibrium, with the weight of the ice mass being balanced by a pressure gradient at the lower surface. Sufficient changes in thickness at or near the grounding line thus define the movement of the grounding line as a result of transition between grounded and floating ice. This movement of grounding line is an important feature in determining the evolution of marine ice sheets, and has been shown to require up to kilometre resolution to resolve adequately (Favier et al., 2014; Cornford et al., 2016).

Numerical modelling of entire continental-scale ice sheets with kilometre resolution and higher-order physics is currently unfeasible due to the high computational cost required. Therefore, to address the need for high resolution in specific parts of the ice sheet while simultaneously limiting the computational cost, BISICLES includes a block-structured adaptive mesh refinement (AMR) method. Using the AMR, the model automatically refines, maintains or coarsens the horizontal resolution in regions as necessary. Resolution can be refined based on stress-balance equations and adjacency to the grounding line and shear margins (Cornford et al., 2013; Favier et al., 2014). The computational efficiency of the model is further enhanced with the capability for MPI-based parallel computing.

The ice thickness h and horizontal velocity vector $\boldsymbol{u}$ satisfy a mass conservation equation for vertically integrated transport of incompressible material, which can be expressed as:

$$\frac{\delta h}{\delta t} = -\bigtriangledown \cdot [\mathbf{u}h] + M_s - M_b, \tag{1}$$

in which M_s is the surface mass balance rate and M_b is the basal melting rate and $\bigtriangledown \cdot [\mathbf{u}h]$ represents horizontal advection of mass.

2.1   Ice flow

The model describes an ice mass evolving through three-dimensional, shear-thinning flow driven by gravity using a depth-integrated ice flow model devised by Schoof and Hindmarsh (2010). The deviatoric stresses and the strain rates are related through a stress balance equation:

$$\bigtriangledown \cdot [\varphi h \mu (2\dot{\epsilon} + 2tr(\dot{\epsilon})\mathbf{I}] + \boldsymbol{\tau}_b = \rho_i g h \bigtriangledown s, \tag{2}$$

in which $\dot{\epsilon}$ is the horizontal strain rate tensor and $\boldsymbol{I}$ is the identity tensor. τ_b is the basal traction (see sections 2.2 and 4.3). $\varphi h \mu$ is the vertically-integrated effective viscosity, and is calculated from the vertically varying effective viscosity μ derived from Glen's flow law, and the stiffening factor φ (Cornford et al., 2015; Nias et al., 2016). The vertically-integrated effective viscosity varies spatially, mainly depending on whether the ice is grounded or not, the basal traction, the ice temperature and how fractured the ice is.

The stiffening factor coefficient φ accounts for variations in several factors including temperature and minor fractures in the ice. For contemporary ice sheets, the stiffening factor is typically solved based on surface ice velocities using inverse methods and is used in the model as an additional tuning parameter when calibrating ice flow to match observations (e.g. Cornford et al., 2015). Due to the lack of direct observations of ice surface velocities for the early-Holocene LIS. We use the default

5 value of $\varphi = 1$ for the entire ice sheet. Given the standard Glen's flow law exponent of $n = 3$, μ satisfies

$$2\mu A(T)(4\mu^2\dot{\epsilon}^2 + |\rho_i g(s-z)\bigtriangledown s|^2) = 1, \tag{3}$$

where z is the depth and $A(T)$ is a rate factor that depends on the ice temperature T through the Arrhenius law (Hooke, 1981).

2.2 Basal processes

10 Boundary conditions at the base of the ice vary between different parts of the ice sheet. Where the ice is floating, there is no basal traction and the normal stress at the base matches the hydrostatic water pressure. Elsewhere the ice is in contact with either bedrock or glacial sediments, of which neither allow flow normal to the base. Following equation 2, the basal traction τ_b is a major controlling factor of the ice flow speed in the model. For ice in contact with bedrock, it can be expressed as:

$$\boldsymbol{\tau}_b = -C|\mu|^{m-1}\boldsymbol{u}, \tag{4}$$

15 with $h(\frac{\rho_i}{\rho_w}) > -r$ as the flotation criteria. C is the basal traction coefficient, which can be set to a spatially varying field and used as a tunable model parameter. τ_b is assumed to satisfy either a non-linear power law, where $m = 1/3$, or a linear viscous relation, where $m = 1$ (with $m = 1$ used in this study). C is typically solved based on the surface ice flow speed using inverse methods for contemporary ice sheets, but for the study presented here, a parametrised field is used based on the abundance and thickness of glacial sediments and bedrock elevation (see section 4.3).

20 A uniform geothermal heat flux of $0.05\ \mathrm{Wm}^{-2}$ is applied at the base of the ice sheet in all of the simulations, with the value based on a geothermal map of North America (Blackwell and Steele, 1992), indicative of a fairly homogeneous geothermal heat flux under the modelled area at present-day (the same value was also used by Gregoire et al., 2012). In the model, the basal heat flux only affects the temperature of the ice, which can impact the ice flow by changing the effective viscosity μ (eq. 3). This is a simplification of the subglacial hydrology, which comprises several processes that can alter the dynamics of

25 ice flow on different time scales (Clarke, 2005; Gladstone et al., 2014). The motion of the base of an ice sheet can be due to (typically plastic) deformation of the underlying sediment or the base of the ice sheet actually sliding on top of the underlying substrate (Gladstone et al., 2014). The sliding is facilitated by the presence and distribution of liquid water at the base, and the yield stress of the deformation of the till is strongly dependent on effective pressure (Iverson, 2010). The conditions at the ice-bed interface (melting or non-melting), availability of liquid water and mechanical properties of the till (soft or hard) thus

30 control the processes that can be activated. These processes are the subject of ongoing developments of the BISICLES model,

but are not included in the version of BISICLES used here. Instead, we emulate the effect of these processes through imposing a spatially variable map of the Basal traction coefficient C.

Basal traction does not impact the flow of floating ice. However, the ice shelves can have a buttressing effect on the ice flow upstream of the grounding line if the shelves are laterally bounded (e.g. Dupont and Alley, 2005). The melting rate under

5 floating ice sheets can thus have a major impact on the flow of ice streams by influencing the buttressing effect (Schoof, 2007). The contemporary Antarctic floating glaciers have been estimated to undergo melt rates in the range of 0–43 ma^{-1} (Rignot and Jacobs, 2002; Rignot et al., 2013). The sensitivity of the modelled ice sheet and the Hudson Strait ice stream to varying rates for this parameter is discussed in section 5.5.

2.3 Calving

10 BISICLES can represent calving in different ways. Here, we use the crevasse calving model of Taylor (2016), which defines the calving front as being where surface or basal crevasses result in a full-thickness fracturing of the terminus. The model calculates the depth of crevasse penetration for the entire domain at both grounded and floating termini. The equations that calculate the penetration depth of both surface and basal crevasses were developed based on earlier studies on calving of tidewater glaciers and marine outlets (Benn et al., 2007a; Nick et al., 2010). A full description of the BISICLES Benn calving model is available

15 in the PhD Thesis of Taylor (2016).

3 Surface mass balance and climate inputs

We simulate the surface mass balance of the Laurentide ice sheet with a PDD surface mass balance model (Rutt et al., 2009) driven by climatological means from a GCM following the same methodology as (Gregoire et al., 2012, 2015, 2016). We drive the PDD model with monthly temperature and precipitation from a series of HadCM3 GCM palaeoclimate 'snapshots' (i.e.

20 equilibrium simulations) run at 1-ka intervals for 26-21 ka and 500-year intervals for 21-0 ka. They are the same simulations used and described in more detail by Morris et al. (2018), Swindles et al. (2018) and Gandy et al. (2018). The snapshots represent a refinement from earlier HadCM3 simulations (Singarayer et al., 2011; Singarayer and Valdes, 2010), and have been updated according to boundary conditions provided for the Palaeoclimate Model Intercomparison Project Phase 4 protocol for simulations of the last deglaciation (version 1; Ivanovic et al., 2016), using the ICE-6G_c reconstruction (Peltier et al., 2015).

25 For the purpose of this work, the climate model output was scaled down to a resolution 0.5×0.5 degrees using a bivariate spline interpolation method. The downscaled resolution is approximately equal to 50×50 km at mid-latitudes. To generate a transient climate forcing, we linearly interpolate between the climate means calculated from the last 50 years of each 500-year snapshot performed for the early Holocene.
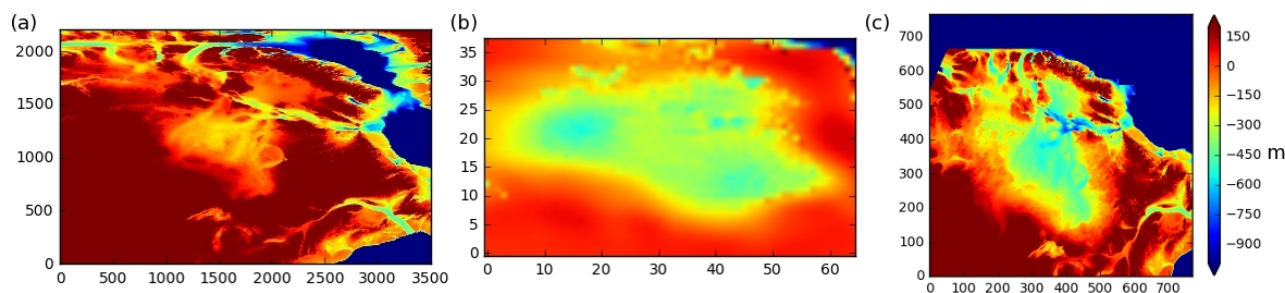
Figure 1. Illustration of the generation of the initial topography. The colour bar indicates the elevation in relation to sea level in metres (m).
(a) The ETOPO1 present day topography relief model of the area around Hudson Bay (adapted from data from Amante and Eakins, 2009).
(b) The difference between the 10 ka and present-day basal topographies in the ICE-6G_c (VM5a) reconstruction (Peltier et al., 2015). **(c)**
The resulting "ETOPO 10 ka" topography map. The basal topography in the northern part of the grid (Greenland and Canadian archipelago)
is set to -1000 m to avoid ice sheet formation in these regions. The coordinates in panels **a** and **b** show the grids in the original datasets, and
the coordinates in panel **c** show the model domain with a 5 km grid.

4 Model setup and experimental design

By the early Holocene, the LIS has significantly retreated from its Last Glacial Maximum position and is far from being at
equilibrium with the climate. Thus, we chose to initialise the geometry of the ice sheet, its thickness and the bedrock topography
based on an available ice sheet reconstruction. We used the ICE-6G_c which has been reconstructed to be consistent with
5 geological records of ice sheet extent, sea level and measurements of modern rates of isostatic adjustment (Peltier et al., 2015).
Ice thickness in this reconstruction is known to be inconsistent with fundamental ice sheet dynamics (Stuhne and Peltier, 2017)
and is also likely inconsistent with the early Holocene climate simulated by HadCM3 because the climate and ice sheet were
not generated in fully (i.e. two-way) coupled framework (e.g. HadCM3 used ICE-6G_c as a boundary condition, but the ice
sheet was not able to subsequently evolve depending on the resulting climate). To account for this inconsistency between the
10 ice sheet and climate, we started our simulations at 10 ka to allow approximately 1500 years for adjustment of the ice sheet
geometry and flow prior to the estimated timing of the separation of the Labrador and Keewatin ice domes (Ullman et al.,
2016), which is the focus of this study.

Several parameters are needed to initialise the model, and they are generally poorly constrained by observations for palaeo
ice sheets. Ice thickness data $h_o(x,y)$, together with surface mass balance $M_s(t,x,y)$ and basal melt rates $M_b(t,x,y)$ are required to
15 initialise the model for solving the equation for conservation of mass (eq. 1). These, together with a map of bedrock elevation
$b(x,y)$, ice temperature field $T(x,y,z)$, basal traction coefficient $C(x,y)$ and an ice stiffening factor $\Phi(x,y)$ allow for solving the
equation of ice flow (eq. 2). The methods used to produce these initial conditions are described in the following subsections.

4.1 Model domain and basal topography

The model domain at the coarsest level Ω^0 consists of a grid of 384×384 rectangular cells of 10×10 km horizontal resolution centred on the Hudson Bay. The projection used is the Lambert Azimuthal Equal Area (LAEA) with a point of origin at 45° N, 95° W, and false easting and northing of 1648.38 km and 202.32 km respectively. The resolution is comparable to what
5   is typically applied in long-term simulations of the modern-day Greenland ice sheet using regular equidistant grids (5-20 km; Goelzer et al., 2017), and what has been used as the base resolution in earlier continental-scale ice sheet simulations using BISICLES (8 km for the Antarctic Ice Sheet in Cornford et al., 2016; 4 km for Greenland in Lee et al., 2015). This base resolution was chosen after initial test runs (not shown here), in which doubling the base resolution to 5 km did not result in significant changes in the ice sheet geometry when keeping the finest resolution allowed in the simulation at 5 km, but resulted
10 in a three-fold increase in the computation cost with the early model setup. The maximum resolution that it is feasible to run the model over this domain for the duration of 2000 years with the current setup is Ω^2 = 2.5 km. An average run speed of 396 model years per day is reached with 96 processors on Tier 3 (ARC3, University of Leeds) high performance computing facilities, whereas test runs with one more level of refinement Ω^3 = 1.25 km slowed the initial run speed to less than 10 model years per day.

15 To produce the bedrock elevation $b(x,y)$, a rectangular bivariate spline interpolation method is used to combine a high-resolution (1 arc-minute resolution) present-day basal topography relief model (fig. 1a, adapted from Amante and Eakins, 2009) with the difference between the 10 ka and present-day basal topographies from the ICE-6G_c reconstruction (fig. 1b). Initial tests were run using the basal topography from the 10 ka time slice of the ICE-6G_c reconstruction, which quickly highlighted the need for finer resolution than the native horizontal grid of the reconstruction (1° × 1°). This was because the
20 blocky structure of the base in ICE-6G_c resulted in unrealistically steep vertical gradients in the surface elevation $s(t,x,y)$. The resulting high-resolution basal topography map is resampled from the swath dataset and projected onto the model grid using a nearest neighbour method to produce the "ETOPO 10 ka" topography map used for initialising the ice sheet model (fig. 1c). The basal topography for the regions of Canadian archipelago and Greenland included in the domain are set to -1000 m to avoid ice sheet build-up in these regions. These areas lack relevance to this study and were excluded in order to save computational
25 cost by avoiding computing the ice velocities there.

The transient isostatic rebound of the crust is not included in the simulations. This feature is available in the UniCiCles model, but including the isostatic rebound in the current model setup reduced the computational performance significantly. As a consequence, the run speed of the model was slowed down by up to 90 % (with Ω^1), making running multiple millennial-scale simulations operationally infeasible. The maximum crustal uplift between 10 ka and the present day in the region has
30 been estimated to be of the order of ~500 m based on the ICE-6G_c reconstruction (fig. 1b; the bedrock under the locations of Labrador and Keewatin ice domes). This could have resulted in the simulated deglaciation being artificially accelerated in some regions, as including the crustal uplift would have resulted in the base of the ice sheet being elevated up to 500 m higher altitudes over the model period.

4.2 Ice thickness and temperature

The thickness of the ice sheet is initialised from the 10 ka time slice of the ICE-6G_c reconstruction using a similar approach to that used for generating the initial topography. The thickness data is first interpolated from low to high resolution (from 1° to 1 arc-minute resolution) using a rectangular bivariate spline interpolation method, and then resampled to the model grid using
5 a nearest neighbour method.

The initial temperature $T(x,y,z)$ of the ice sheet is taken from the 9 ka time-slice of a previous LIS deglaciation simulation using the GLIMMER-CISM ice sheet model (Gregoire et al., 2012). The original data is on a LAEA grid with a common point of origin with my experiment (45° N, 95° W), but with a larger domain covering most of North America (the GLIMMER-CISM study examined the evolution of the whole North American Ice Sheet over the last glacial cycle). The data is interpolated to
10 the smaller domain and higher resolution using the rectangular bivariate spline interpolation method. The 9 ka time slice of the previous study was chosen because it presents a close fit to the extent of the ICE-6G_c ice sheet at 10 ka, which is the starting point of the transient simulations presented here. The two do not match exactly, and for grid cells where the reconstruction indicates that ice should be present but the GLIMMER-CISM simulation is ice-free, the temperature is initialised to 0 °C for all vertical levels. This was chosen to encourage melting of the extensive thin areas of the initial ice sheet. The empirical
15 relationship of area to volume ratios of contemporary ice sheets (fig. 4 in Ullman et al., 2016; Paterson, 2016) suggests that the LIS in ICE-6G_c at 10 ka is likely too extensive at $6.08 \cdot 10^6$ km^2, which is significantly larger than the area expected based on the reconstructed volume ($6.81 \cdot 10^5$ km^2).

4.3 Basal traction and ice stiffening factor

Basal traction is a major factor determining the ice flow in BISICLES (eq. 2), and one of several factors that have been
20 identified as potential controls for ice flow and streaming locations in ice sheets (Winsborrow et al., 2010; Stokes et al., 2016). The presence of water and thickness of subglacial sediments have an influence on the basal traction, as till deformation can accelerate basal flow. This has been shown to be important for the ice dynamics in earlier modelling studies of the LIS (Marshall et al., 2002; Tarasov and Peltier, 2004). The version of BISICLES we used here does not yet include processes of basal hydrology that are needed to generate ice streams. We thus adjust the basal traction coefficient $C(x,y)$ to account for these
25 effects as is typically done in simulations of modern ice sheets. To represent this dependency of basal traction on subglacial properties and to determine the basal traction coefficient $C(x,y)$ for these simulations, the domain was divided into three different types of grid cells according to sediment coverage. The division was based on a geological map of North America by Reed et al. (2005), and shown in fig. 2a.

In addition to the underlying substrate, Basal topography and topographic troughs are a major factor influencing the gen-
30 eration and positioning of ice streams (Paterson, 2016; Winsborrow et al., 2010). This effect was incorporated by relating the basal traction coefficient C for the regions of bare bedrock as a function of bedrock elevation b using:
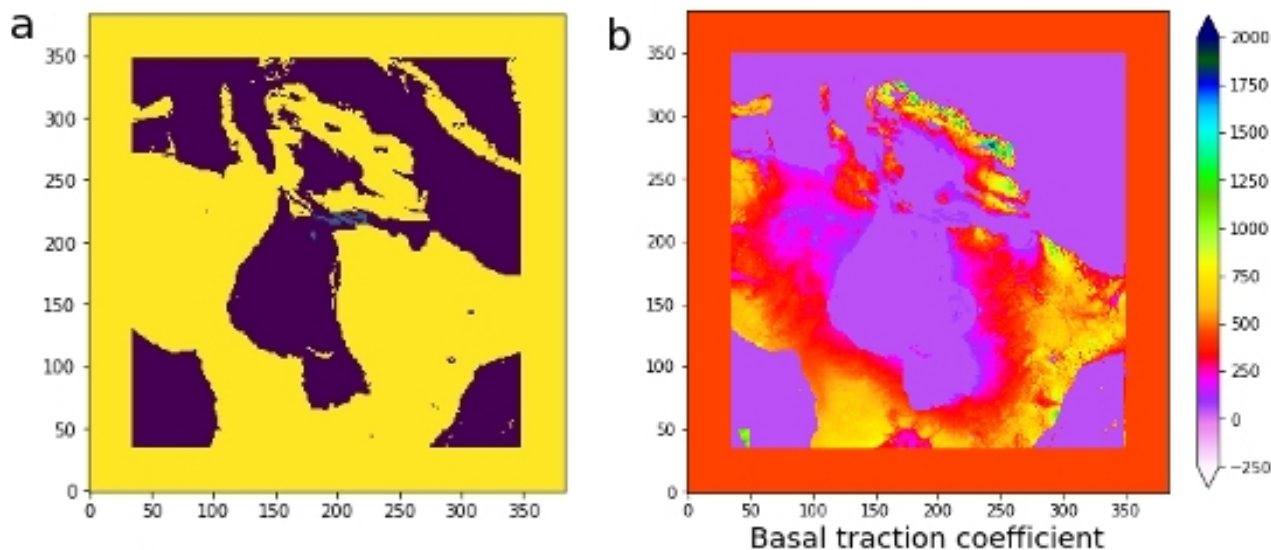
$$C(x,y) = b(x,y)C_i + C_{sl}, \tag{5}$$

Figure 2. Panel **(a)** shows the domain divided into three different types of sediment coverage: bare bedrock, sediment-covered and submerged bare bedrock in the Hudson Strait, with the grid cells coloured yellow, dark blue and green respectively. The division is based on the geological map of North America presented by Reed et al. (2005). **(b)** Basal traction coefficient map used in the '*standard*' simulation, for which the basal traction coefficient (C) values are calculated based on bedrock elevation and sediment coverage.

where C_i is the increment of the basal traction coefficient with elevation (0.3 m^{-1} in the '*standard*' simulation), and C_{sl} is the value for bedrock at sea level ($C = 500$ Pa m^{-1} a in '*standard*').

A fixed value is used in areas with a sediment coverage (figure 2). The range of C -values chosen for the initialisation was based on values from modern-day simulations of the West Antarctic Ice Sheet using BISICLES (with the same linear viscous relation of $m = 1$ as in this study), for which basal traction coefficients were inversed from ice surface velocity data (Cornford et al., 2015). These values are detailed in Section 5.

4.4 Surface mass balance and basal fluxes

The model defines the SMB using the PDD scheme described in section 3. Values of 4.5 and 12 mm d^{-1} $^{\circ}$C^{-1} were chosen respectively for the PDD factors of snow and ice while setting up the '*standard*' simulation. These values are 50% higher than the typically used values of 3 and 8 mm d^{-1} $^{\circ}$C^{-1}, and were chosen by manual tuning for the '*standard*' as a stronger ablation is necessary for the LIS to deglaciate in accordance with the reconstructed ice extent (Dyke, 2004). The need for higher PDD factors was apparent as the ice sheet underwent substantial growth in the early simulations that employed the typical PDD factors, and the total volume of the ice sheet was still higher than the initialised ice volume after 1500 years of simulation. Using the PDD method has been highlighted as challenging for modelling the SMB of palaeo ice sheets (Bauer and Ganopolski, 2017; Charbit et al., 2013; Van de Berg et al., 2011), with one major problem being that the method does not explicitly account

for the absorption of shortwave radiation (e.g. Van de Berg et al., 2011). The fixed PDD factors also do not take into account the temporal and spatial variability in insolation, cloud optical properties, snow properties, snow density, water content in snow and changes in albedo, among other assumptions (Charbit et al., 2013). Following this, recent research has suggested that using the standard values is unlikely to predict the melt rates correctly under climatic conditions that differ from those in

5 present-day Greenland (Bauer and Ganopolski, 2017; Charbit et al., 2013; Van de Berg et al., 2011). Bauer and Ganopolski (2017) recently compared the use of a physically-based surface energy balance method and the PDD method for simulating the North American Ice Sheet over the last glacial cycle, and found PDD factors of 9 and 16 mm d^{-1} $°C^{-1}$ respectively for snow and ice to produce the best results for 15 ka conditions (the study did not provide an estimate for a time period closer to the timing of the Hudson Bay saddle collapse). Moreover, exactly what the 'best' values for the PDD factors are is dependent on

10 the model setup, which highlights the importance of assessing this parametric uncertainty through a sensitivity study.

The lapse rate γ is set to 5 $°C$ km^{-1} following the experimental setup of Gregoire et al. (2012). The value is based on the numerical modelling work of Abe-Ouchi et al. (2007) who found it more appropriate for the North American ice sheet than the typically used range of 6–8 $°C$ km^{-1}.

The basal heat flux is set to a constant 50 mW m^{-2} following the methodology of Gregoire et al. (2012), which ensures

15 consistency with the initial ice temperature fields (also taken from the same study). They chose the value based on a geothermal map of North America (Blackwell and Steele, 1992), which is indicative of a fairly homogeneous modern geothermal heat flux under the modelled area. The value is of similar magnitude to modern-day geothermal heat flux under the Antarctic ice sheet, which has recently been suggested to vary between 42–180 mWm^{-2}, with a mean of 68 mW m^{-2} (Martos et al., 2017). If all of the available heat from the basal heat flux of 50 mW m^{-2} would result in ice melt, the base of the ice would melt at a rate

20 of ~5 mm a^{-1}. Since even this extreme value is 2–3 orders of magnitude smaller than the surface melt rates, we assume for the purposes of this study that it is negligible and the basal melting rate is set to 0 m a^{-1} in all simulations.

For the sub-shelf melt rate, we chose a standard value -15 m a^{-1}. This is comparable to areas of high sub-shelf melt around modern-day Antarctic Ice Sheet, where the rates have been estimated to be up to ~43 m a^{-1} (Rignot et al., 2013). The higher end of this range was chosen due to the orbital configuration of the Earth approaching the Holocene Climatic Optimum conditions

25 post 10 ka (Kaufman et al., 2004), and the associated increase in radiative forcing could have resulted in substantial heat absorption to the lake and sea water adjacent to the ice sheet. Sub-shelf melt rates have been shown to be strongly positively correlated with increasing ocean temperatures, with a relationship of ~10 m K^{-1} estimated from radar interferometry-based observations of basal melt rates seaward of Antarctic grounding lines and nearby in-situ ocean temperature measurements (Rignot and Jacobs, 2002). Using a single value for the sub-shelf melt over the whole model period is a simplification of the

30 process, whereas in reality the temperature of water in contact with the ice shelf likely underwent changes over the 10–8 ka period. Accurately estimating the sub-shelf melt rate at the marine margin of the LIS over time is, however, challenging due to a lack of quantified adn spatially detailed proxy records of Sea Surface Temperatures (SSTs) and the location of the ice margin being uncertain over time due to limited records constraining the retreat (Dyke, 2004). An alternative approach would have been to estimate the sub-shelf melt using the above relationship between the melt rate and the SST from the climate

35 model output. The modern-day Antarctic melt rates were preferred due to the low horizontal resolution of the climate model

simulations we use (1.25 × 1.25 degrees in the ocean and 3.75 × 2.5 degrees in the atmosphere). The oceanic grid cells adjacent to the ice margin at 10 ka cover an area of ~$0 \cdot 10^4$ km^2 of the Labrador Sea, and are thus not representative of the SST at the comparatively narrow ice margin.

5   Ice sheet sensitivity to model parameters

5   The evolution of ice sheet thickness, volume and melt in the model is dependent on the choices of input model parameters. To gain a better understanding of which parameters control the rates of LIS deglaciation and the magnitude, duration and timing of the Hudson Bay saddle collapse, a series of sensitivity simulations were performed. The simulation labelled 'standard' is used as the starting point for varying individual parameters, and the parameters are varied systematically, one at a time. This approach allows for examining the effects of adjusting individual parameters while keeping the rest constant. This is

10   particularly important because BISICLES has not previously been used in a palaeo context for the Laurentide Ice Sheet, where these values cannot be obtained using direct observations or inverse methods. Two simulations were run to assess the sensitivity to each of the 5 model parameters, resulting in a total of 11 simulations with the model parameters and their respective ranges shown in Table 1. To evaluate the impact of the transient climate and the spin-up adjustment period, a 'control' simulation with a constant 10 ka climate and 'standard' set of parameter values was also included.

Table 1. Model parameters varied in the study and their ranges, with 'standard' values (as discussed in section 4) shown in brackets.

Parameter	Symbol	Value ('standard')	Unit	Reference
Levels of refinement	Ω^{0-2}	10–2.5 (5)	km (grid size)	4.1
Basal traction	C	1-6×'standard'	Pa m^{-1} a	4.3
PDD factor for snow	α_s	3–6, (4.5)	mm (d $^\circ$C)$^{-1}$	4.4
PDD factor for ice	α_i	8–16 (12)	mm (d $^\circ$C)$^{-1}$	4.4
Sub-shelf melt rate	M_{ss}	2–45 (15)	m a^{-1}	4.4
Precipitation	P	0.5–1×'standard'	kg m^{-2}	3.2

15   ### 5.1   Laurentide Ice Sheet evolution in 'Standard' and 'control' simulations

This subsection describes how the ice sheet evolves in the 'standard' simulation. Figure 3 shows the ice sheet at model year 50 as it is still adjusting to the initial conditions. The ice thickening rate (fig. 3b) has a mean of -0.20 m/a and a range of -94.25–37.26 m/a, and the modelled ice velocity field (fig. 3c) shows velocities of up to ~5 km/a at the mouth of the Hudson Strait and the modern Ungawa Bay region. The initial adjustment period is dynamic and results in a substantial reorganisation

20   of ice, which is largely a result of the chosen initial ice thickness field from ICE-6G_c not being physically consistent with

the dynamical BISICLES ice sheet model as discussed in section 4.2. The ICE-6G_c includes "unphysical geometric details" (Stuhne and Peltier, 2017), because the reconstruction is built from glacial isostatic adjustment (GIA), LIS extent data (Dyke, 2004), a model of viscoelasticity (VM5a) and eustatic sea level record for estimating the volumetric distribution of the ice mass (Peltier et al., 2015). Therefore, this adjustment of our simulated ice sheet is both necessary and expected. The surface mass

5   balance is positive over the majority of the ice sheet (fig. 3d), with a mean of 0.25 m/a and a range of -11.52–1.29 m/a.
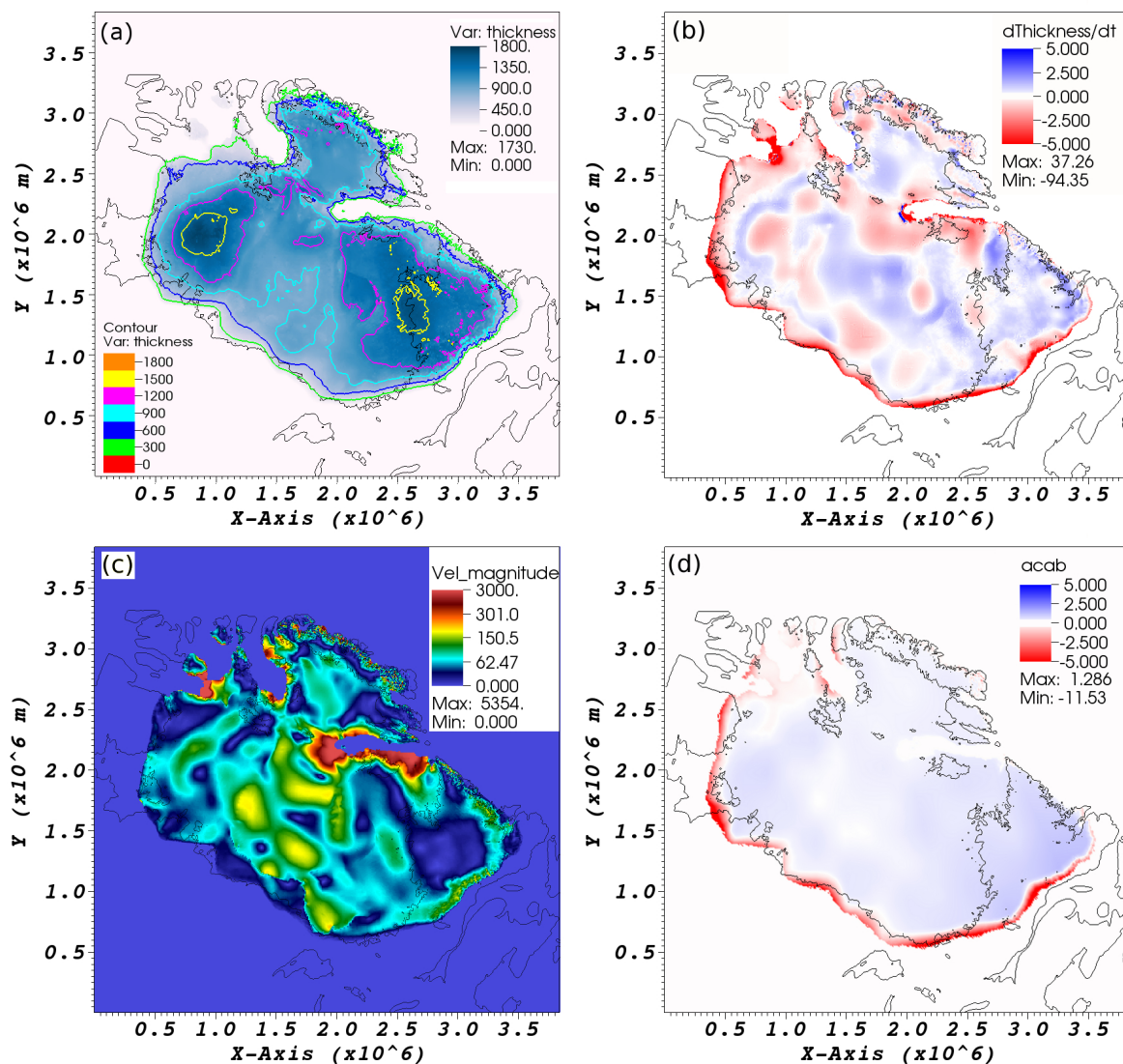
Figure 3. 'Standard' simulation at model year 50. Panels show **(a)** ice thickness with 300 m contour lines, **(b)** ice thickening rate $\frac{dh}{dt}$ (m/a), **(c)** magnitude of the vertically integrated ice velocity (m/a), **(d)** surface mass balance (accumulation - ablation; m/a.)

The volumetric loss and the elevated freshwater flux (FWF) over the first ~100 years in both 'control' and 'standard' simulations (fig. 4) simulations is a result of the modelled ice sheet undergoing dynamical reorganisation after initialisation and initially high ice melt rate of the extensive parts of the ice sheet, mainly on the southern and northwestern parts of the simulated LIS (fig. 5). The subsequent increase in 'control' ice volume shows that the ice sheet is not in equilibrium with

5 the 10 ka climatic forcing. The evolution of the volume above flotation in the 'standard' simulation differs from the negative trend in the volumetric evolution of the LIS in the two reconstructions shown in fig. 4, where the 'standard' simulation is compared to the ICE6G_c and GLAC-1D reconstructions. The volumetric change over 10–8 ka in the ICE-6G_c and GLAC-1D reconstructions are on average 0.34 m per 100 years and 0.50 m per 100 years respectively, and indicative of a continual decrease in volume over the time period. The evolution of the ice volume in the 'standard' simulation is indicative of the

10 ablation and dynamic export of ice being balanced by accumulation for the first 1000 model years, during which the simulated LIS volume above flotation decreases by approximately 7%.
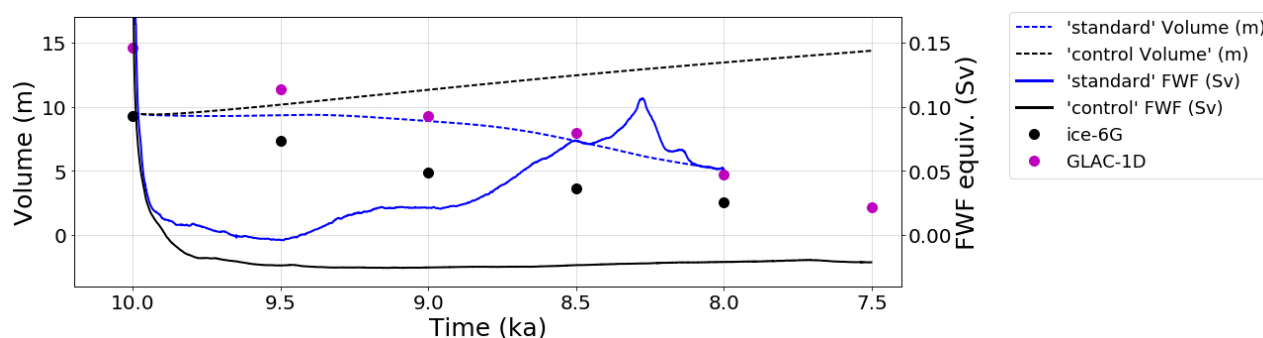

Figure 4. Evolution of ice sheet volume in metres of sea level rise equivalent (dashed line) and freshwater flux (FWF) equivalent in Sverdrups (solid lines). The volumetric SLR equivalent of the ice sheet is calculated from the volume above flotation, and the FWF from the total volumetric change between model years. The volume and FWF in the 'standard' simulation are shown in blue, and for the 'control' simulation in black. The black and magenta markers show the volume in metres of equivalent SLR in the ICE-6G_c (VM5a; Peltier et al., 2015), and the GLAC-1D (Tarasov et al., 2012) reconstructions.

The total volumetric change in the 'standard' simulation converted into FWF (solid blue line in fig. 4), shows a period of accelerated melt from model year 1321 onwards, with the melting defined as accelerated in the simulation over periods when the FWF value is higher than 0.05 Sv (the value used for the background meltwater flux in Matero et al., 2017). The FWF

15 reaches its peak value of 0.106 Sv during a 200 -year period of acceleration from model year 1637 onwards, and corresponds to the separation of the Labrador and Keewatin ice domes. The simulated separation of the ice domes occurs at a similar time to the scenarios in Matero et al. (2017), in which the peak FWF was released at a time corresponding to approximately 8.25 ka. This is close to the timing that freshening signals from North Atlantic sediment cores suggest that the largest release of meltwater from the LIS would have taken place (~8.49 ka or ~8.29 ka, Ellison et al., 2006; ~8.38 ka, Kleiven et al., 2008;

20 ~8.5 ka, Lochet et al., 2019). The timing and duration of the modelled saddle collapse in 'standard' are thus similar to some of our scenarios in Matero et al. (2017). However, the total SLR equivalent of the released FWF in 'standard' over the 200
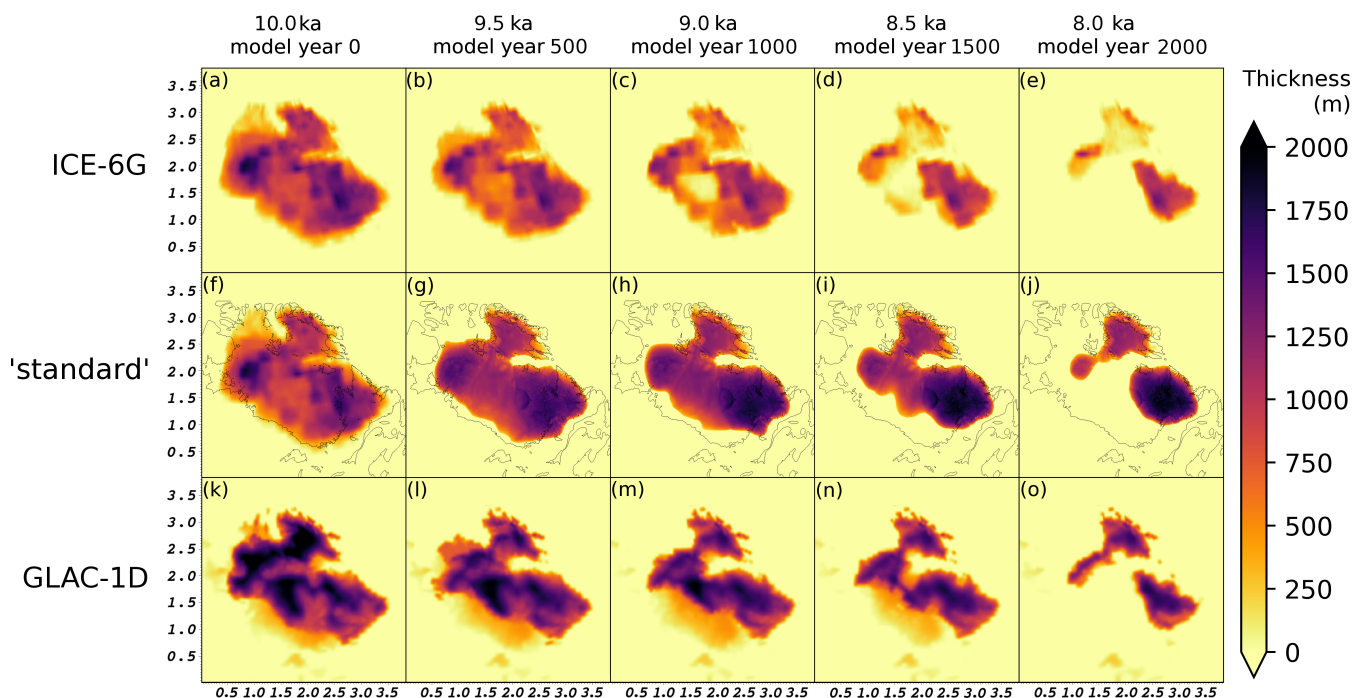
Figure 5. Ice sheet thickness evolution in the ICE-6G_c (VM5a; Peltier et al., 2015) reconstruction in panels **(a)**–**(e)**, the 'standard' simulation in panels **(f)**–**(j)** and the GLAC-1D reconstruction (Tarasov et al., 2012) in panels **(k)**–**(o)**. The ice thickness in each series is plotted in 500 year intervals. The coastlines plotted in panels **f**–**j** are based on the "ETOPO 10 ka" topography described in section 4.1.

-year period is 1.57 m, which is approximately 46% of the 3.39 m attributed to the saddle collapse period in the 4.24m_200yr scenario in Matero et al. (2017). Nonetheless, the simulated volumetric ice loss is close to the rate of volumetric change in the GLAC-1D ice sheet reconstruction over a wider 500-year window; 3.3 m of SLR equivalent from 8.5 to 8.0 ka (fig. 4).

The major changes during the first 1000 model years in 'standard' are a ~37 % decrease in the ice extent from $6.08 \cdot 10^6$ km^2
to $3.86 \cdot 10^6$ km^2, and a reorganisation of the ice mass resulting in thickening of the ice sheet at the ice saddle and Labrador ice dome, and a thinning of the Keewatin ice dome (fig. 5f–j). It is also interesting to note that by model year 1000 (corresponding to 9 ka), the modelled ice sheet in 'standard' adjusts itself to resemble the GLAC-1D reconstruction more than the ICE-6G_c reconsutrction in terms of volumetric evolution (fig. 4), shape and extent (fig. 5), despite the simulation initially being set up using the ICE-6G_c configuration. This is likely due to the climatic influence on ice sheet evolution and the dynamical aspects of the BISICLES and GLAC-1D models, suggesting that these are important components for accurate representation of palaeo ice sheets.

One feature that particularly stands out as being different between the simulated ice sheet (fig. 5h) and the ICE-6G_c recon-struction (fig. 5c) by model year 1000 (9 ka) is the thickness of ice over central Hudson Bay, which is the ice saddle connecting the Labrador and Keewatin ice domes. The GIA-based reconstruction indicates that the ice sheet would have deglaciated 'inside out', with the central part being free of ice before the surrounding regions. This pattern of deglaciation is not reproduced in any

of the BISICLES simulations or the GLAC-1D reconstruction (fig. 5m). The difference in the volumetric change between the simulated ice sheet and the ICE-6G_c reconstruction (fig. 4) is largely a result of differences in reconstructed and modelled ice thickness over the Labrador and Foxe ice domes. These differences are clearest between year 8 ka in the reconstruction (fig. 5e) and model year 2000 (fig. 5j), with the modelled ice thickness having a maximum of 2188 metres at the Labrador dome

5 and just over 1200 metres for ICE-6G_c.

5.2 Impact of varying the mesh resolution

This subsection describes the results of increasing and decreasing the level of refinement of the adaptive mesh. Simulation 'AMR_0' had 0 levels of refinement (10×10 km resolution, Ω^0), 'standard' had 1 level of refinement (up to 5×5 km resolution, Ω^1) and 'AMR_2' had 2 levels of refinement (up to 2.5×2.5 km resolution, Ω^2). Running the current setup with 3

10 levels of refinement proved infeasible computationally, as run speeds decreased dramatically from ~50 model years per hour (2 levels of refinement) to 1 model year per day (3 levels of refinement), and thus this part of the sensitivity study was limited to 2 levels of refinement.

Increasing the level of refinement of the AMR from Ω^0 to Ω^2 does not have nearly as big an impact on the long-term rates of change in volume (fig. 6a), as has been reported in a study of the West Antarctic Ice Sheet using BISICLES (Cornford

15 et al., 2016), for example. Cornford et al. (2016) used a base resolution of 8 km, and increasing the refinement to 4 km or 2 km grid size resulted in distinct rates of change (see fig. 2 in Cornford et al., 2016), highlighting the necessity for using high resolution for simulating marine ice sheets. Based on these initial simulations it seems that such high resolution is not as critical between these levels of refinement for the LIS deglaciation, which is has a smaller marine or lake-terminating margin than West Antarctica (fig. 6a). These results do not, however, preclude the potential for differing patterns of deglaciation with

20 further refinement (and alternate boundary conditions). Increasing the level of refinement from Ω^1 to Ω^2 results in the peak FWF occurring 19 years earlier, and decreasing the level of refinement from Ω^1 to Ω^0 results in the peak FWF occurring 4 years later. The durations and peak values in the discharge are similar between the three simulations, at 0.107, 0.107 and 0.106 Sv for 'AMR_0', 'standard' and 'AMR_2' respectively. The timing of the peak FWF in these simulations differs mainly between model years 1550 and 1890, which coincides with the deglaciation of the part of the ice sheet connecting the Keewatin and

25 Labrador domes over Hudson Bay (the saddle collapse).

At model year 1700, the ice flow on both sides of the ice saddle is faster in the 'AMR_2' simulation compared to the 'standard', and the grounding line on the northeastern side has retreated approximately 41 km further towards the centre of the ice saddle. After model year 1890 the rate of change returns to similar values between the simulations, suggesting that the high resolution is more important for the more dynamical periods of the LIS deglaciation (such as the saddle collapse). This is

30 in contrast to periods of deglaciation mainly driven by surface ablation.

Increasing the model resolution results in a faster retreat of the grounding line and has an impact on the timing of the peak FWF, with the differences in timing diverging with higher levels of refinement. The resolution of the mesh is thus an important parameter to investigate in terms of understanding the saddle collapse. Increasing the level of refinement could further alter the deglaciation pattern of the ice saddle and ice streams.
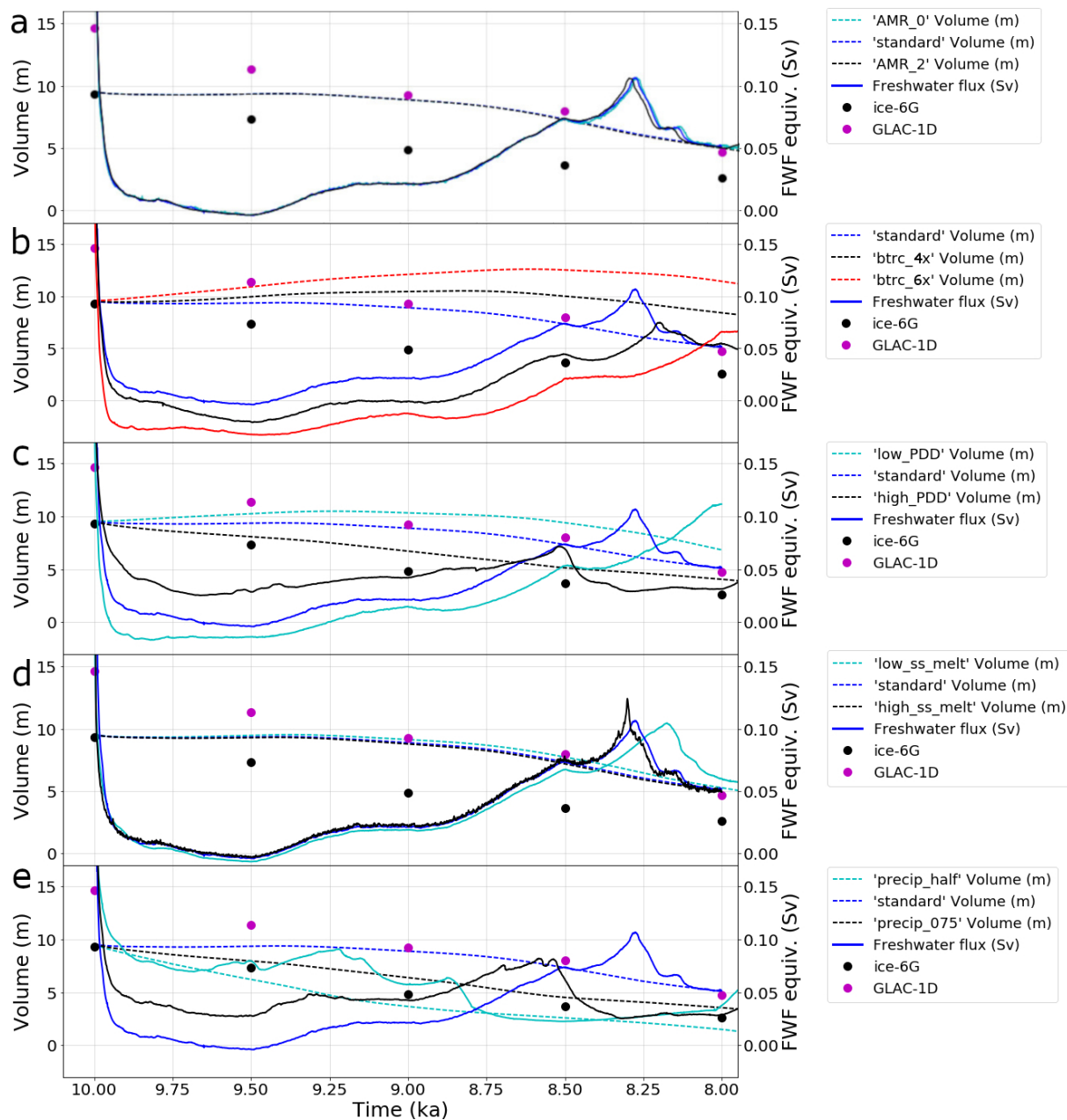
Geoscientific
Model Development
Discussions

Open Access

EGU

Figure 6. Effects of varying **(a)** adaptive mesh resolution, **(b)** basal traction coefficient C, **(c)** PDD (positive-degree-day coefficients), **(d)** sub-shelf melting rate and **(e)** precipitation on simulated ice sheet volume in meters of sea level rise equivalent, and freshwater flux equivalent in Sverdrups. The black and magenta markers show the volume in metres of equivalent sea level rise (SLR) in the ICE-6G_c (VM5a; Peltier et al., 2015), and the GLAC-1D (Tarasov et al., 2012) reconstructions.

5.3 Impact of varying the basal traction coefficient

The basal traction coefficient C in the 'standard' simulation is defined as shown in fig. 2b, and C-values are set to 50 Pa m^{-1} a for the sediment-covered regions, and to 80 Pa m-1 a for the regions with submerged bedrock at the mouth of Hudson Strait. The C-values for the bedrock regions are defined as 400 Pa m-1 a at sea level (z=0 m), and increase with the elevation of

5   the bed at a rate of 150 per 500 Pa m^{-1} a. In the 'btrc_4x' simulation the C-values and rate of change with elevation of the bed are quadrupled from the 'standard' values (and multiplied by 6 in the 'btrc_6x' simulation). The resulting C-ranges in the three simulations are 0–939 Pa m^{-1} a, 0–3756 Pa m^{-1} a and 0–5634 Pa m^{-1} a for 'standard', 'btrc_4x' and 'btrc_6x' respectively. The effect of halving the basal traction coefficient values from 'standard' was also tested. This effectively makes the ice sheet base very slippery and causes the model to crash after 15 years due to extreme ice velocity acceleration that

10 becomes unsolvable.

Increasing the basal traction between the simulations results in a near-uniform deceleration of the ice flow shortly after initialisation, which in turn slows down the export of ice from the domes and the transport of ice towards the ice margins. This, in combination with the high accumulation rates in the simulations, initially results in glaciation instead of deglaciation for the 'btrc_4x' and 'btrc_6x' simulations (red and black lines in fig. 6b). The peak freshwater flux in 'btrc_4x' also occurs

15 50 years later (and 250 years later in 'btrc_6x') with smaller magnitudes and longer durations for the elevated meltwater flux compared to the 'standard' simulation. Panels **a–c** in fig. 7 show the ice thickness at model year 1750 in each of the simulations, demonstrating that increasing the basal traction coefficient value results in thicker and more extensive ice domes.

The resulting ice velocities are, however, high in 'standard' compared to modern velocities for the Antarctic ice sheet (e.g. Rignot et al., 2011, 2008; Rignot and Kanagaratnam, 2006) and in Greenland (Rignot and Kanagaratnam, 2006). This is likely

20 a result of the basal traction coefficient values in 'standard' being smaller than those solved using inverse methods for use with BISICLES for the modern West Antarctic Ice Sheet (Cornford et al., 2015). These earlier studies and the fact that the ice velocities in 'standard' are approaching the threshold of unrealistic ice velocities, suggest that the basal traction coefficient values used in these simulations could have been set to be too low to compensate for the high rates of ice accumulation. Another reason for the high velocities could be high stress and strain rates that result from the initial shape and surface slope gradients

25 of the ice sheet being at least initially too steep, having been initialised from the GIA-based ICE-6G_c reconstruction.

At model year 1000, there is still fast-flowing ice present at all three domes, with integrated velocities in the range of 10^2 m/a. This magnitude is more characteristic for contemporary outlet glaciers in the Greenland Ice Sheet (Rignot and Kanagaratnam, 2006), but the LIS was experiencing rapid deglaciation at the time, and it is feasible that the ice flow rates towards the periphery were high. The presence of meltwater during the melting season has been shown to accelerate ice flow in the Greenland ice

30 sheet (the "Zwally effect"; Zwally et al., 2002), and meltwater was likely extremely abundant during the surface-melt driven retreat of the LIS (Carlson et al., 2009). For comparison, the background FWF used in Matero et al. (2017) to represent the melting of the LIS outside the saddle collapse period was ~16 times the freshwater flux of 0.003 Sv from the contemporary Greenland ice sheet (Shepherd and Wingham, 2007), and this does not include the meltwater pulse from the Hudson Bay ice saddle collapse.
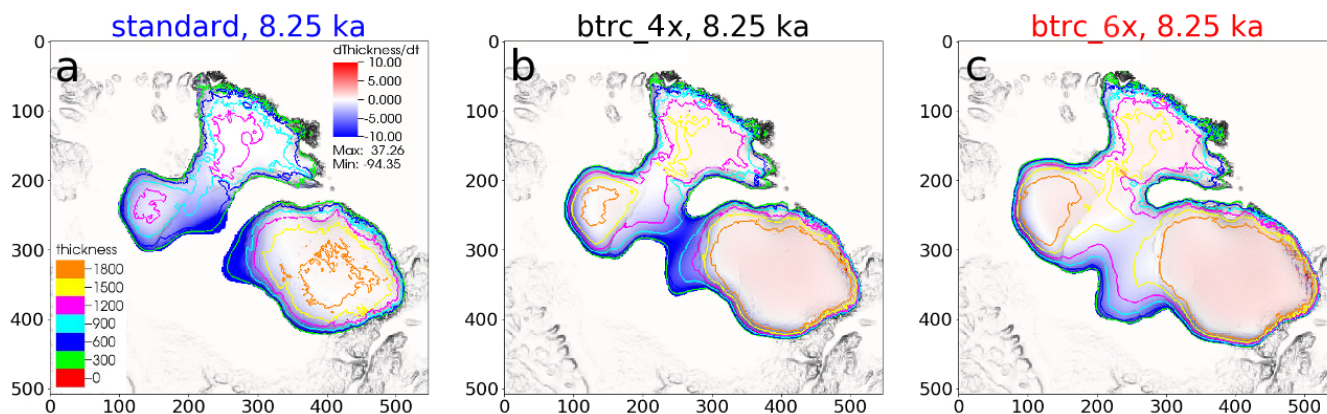
Geoscientific
Model Development
Discussions

Figure 7. Modelled ice thickness and rate of change of thickness (m/a) at model year 1750 in (a) the 'standard' simulation, (b) the *btrc_4x*
simulation in which the standard basal traction coefficient field is quadruple, and (c) *btrc_6x* in which the standard basal traction coefficient
field is multiplied by 6.

5.4 Impact of varying the PDD factors

The PDD factors in the '*standard*' simulation are set to $\alpha_s = 0.0045$ mm d^{-1} °C^{-1} for snow and to $\alpha_i = 0.012$ mm d^{-1} °C^{-1}
for ice. Simulation '*low_PDD*' has lower PDD factors of $\alpha_s = 0.003$ mm d^{-1} °C^{-1} and $\alpha_i = 0.008$ mm d^{-1} °C^{-1}, and for
simulation '*high_PDD*' these were set to $\alpha_s = 0.006$ mm d^{-1} °C^{-1} and $\alpha_i = 0.016$ mm d^{-1} °C^{-1}.

5   Since the other climatic parameters are the same between the simulations, the initial impact of changing the PDD factors was
expected to be fairly straightforward, with higher values resulting in more pronounced melting, which fig. 6c demonstrates. The
surface melt rates in simulations with higher PDD factors include two important positive feedbacks for individual locations.
Firstly, faster melting of the snow cover due to an increase in α_s has the compounded effect of accelerating the total surface
melt once the snow cover melts completely due to α_i having a larger value than α_s. Secondly, surface melt leads to lowering
10   of the surface, which further accelerates the melting through local increase in the surface air temperature in accordance with
the SAT lapse rate Γ.

The higher PDD factors in '*high_PDD*' compared to the '*standard*' result in the peak freshwater flux and the saddle collapse
occurring 225 years earlier (fig. 6c), with a lower magnitude (0.07 Sv and 0.11 Sv respectively, fig. 6c). The separation of the
Keewatin and Labrador ice domes in '*low_PDD*' is delayed by over 275 years compared to the '*standard*' simulation, and fig.
15   8a shows the ice sheet at the end of the simulation.

The different PDD factors between the simulations cause distinctly different patterns for the evolution of the ice volume
above flotation in the simulations (fig. 6c). Over the first 1000 model years, the volume in meters of sea level rise equivalent
increases by ~8% in '*low_PDD*', decreases by ~8% in '*standard*' or decreases by 30% in the '*high_PDD*' simulation, making
the model setup highly sensitive to the value chosen for this parameter. '*high_PDD*' is the first of the simulations presented here
20   that is approaching a rate of volumetric change that is comparable to that of ICE-6G_c, in which the LIS volume decreases by an
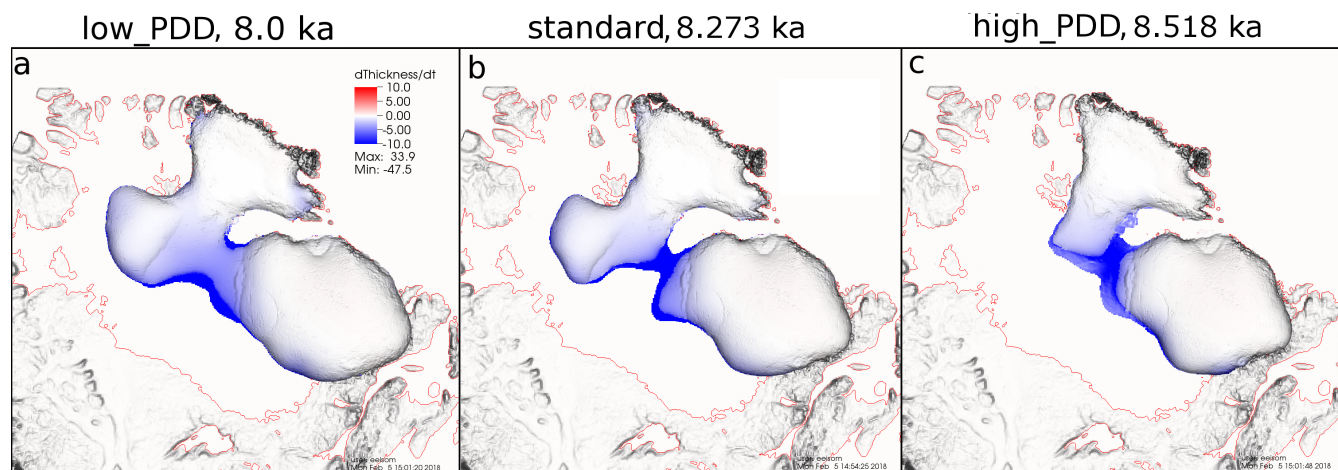
Figure 8. Ice sheet at the time of the peak freshwater flux in the **(a)** 'low_PDD' simulation, **(b)** 'standard' simulation, **(c)** 'high_PDD' simulation. The separation of the Keewatin and Labrador domes in the 'standard' and 'high_PDD' simulations is at a more advanced stage at the time of peak freshwater flux compared to the 'low_PDD' simulation. The freshwater flux in 'low_PDD' would likely have increased as the separation of the ice domes would have continued if the simulation was run for longer than 2000 model years.

average of ~0.33 metres of SLR equivalent every 100 years for the period between 10 ka and 8 ka (0.28 m of SLR equivalent per 100 years in '*high_PDD*'). In GLAC-1D, the average volumetric loss over the 2000 year period is approximately 0.50 metres of SLR equivalent per 100 years, which is 80% larger than the ice loss rate in '*high_PDD*'. It is worth noting that the two are not directly comparable due to the different initial ice sheet geometries and ice volumes. The initial ice volume
5 in '*high_PDD*' is approximately two thirds of the volume in GLAC-1D at 10 ka, with the GLAC-1D ice sheet being thicker over a comparable extent (figures 5f & 5k). Both reconstructions indicate a more rapid fractional loss over the period than the BISICLES simulations presented here (fig. 6c), and in all three of our simulations, the Labrador dome is a stable feature and a constant store of freshwater by model year 2000 (~3.71 *m*, 4.50 *m* and 4.58 *m* of SLR for '*high_PDD*', '*standard*' and '*low_PDD*' respectively).

10 **5.5   Impact of varying the sub-shelf melting rate**

Three values for sub-ice shelf melting rate (M_{ss}) were tested in order to evaluate the sensitivity of the early-Holocene LIS deglaciation to this parameter: 5 m/a ('*low_ss_melt*'), 15 m/a '*standard*' and 45 m/a '*high_ss_melt*'. Representing the sub-shelf melt with a single value over a 2000 -year period is a simplification, as it is a process varying both in time and space even for individual ice shelves. An example of the possible spatial variability is a study by Rignot and Steffen (2008), who found
15 the sub-shelf melt rate under Petermann Glacier in Northern Greenland to be highly channelised along the flowline, reaching between 0–25 m/a over the 2002–2005 period. Seasonal variability, and whether the ice front at the marine terminus is an extensive ice shelf or a vertical calving front also has an impact on submarine melt rates. Indeed, individual tidewater glaciers have been estimated to undergo periods of extremely high summer melt at 3.9 ± 0.8 m/day in Western Greenland (Rignot et al.,

2010) and up to 12 m/day at the Leconte Glacier in Alaska (Motyka et al., 2003). A source of uncertainty in these simulations is treating the lacustrine front on the southwestern side of the LIS (i.e. Lake Agassiz) with the same values for basal ice sheet melt as the marine margins. The Lake Agassiz sub-shelf melt is currently difficult to constrain due to both the volume and extent of the lake being uncertain over time (Leverington et al., 2002; Clarke et al., 2004) and no studies have been published

5   on the potential heat budget of the lake and its interactions with the LIS.

The time series of change in volume between the two simulations with larger sub-shelf melt values ('*standard*' and '*high_ss_melt*') are similar until model year 1650, when larger regions of the ice saddle connecting the Labrador and Keewatin domes thin sufficiently to become afloat (fig. 6d). Following this, the deglaciation of the central Hudson Bay in '*high_ss_melt*' becomes accelerated in comparison to '*standard*', resulting in a peak meltwater flux of 0.124 Sv that occurs 24 years earlier than the

10   peak flux of 0.107 Sv in '*standard*'. The difference in timing of the peak meltwater discharge between the '*low_ss_melt*' and '*standard*' simulations is larger (101 years), but the values of peak discharge between the two simulations are very similar. In addition to being delayed, the saddle collapse meltwater pulse in '*low_ss_melt*' has a longer duration.

For the majority of the 2000 -year simulation the rate of volumetric change of the LIS is not sensitive to varying the sub-shelf melt, but the parameter becomes important during the more dynamical part of the deglaciation once parts of the ice sheet

15   over Hudson Bay thin sufficiently to begin to become afloat. The rate of meltwater flux in '*low_ss_melt*' starts to deviate from that of the two simulations with higher sub-shelf melt rates after model year ~1280, which is likely due to the ice shelves in '*low_ss_melt*' exerting a stronger buttressing effect on the ice flow and export across the grounding lines at the marine margins. An interesting piece of future work could be to study the importance of sub-shelf melt rates together with increasing the model resolution to sub-kilometre grid cell size, and to examine the changes in the Hudson Strait ice stream and movement of the

20   grounding line there.

5.6 Impact of varying the precipitation rates

The input climatologies to the ice sheet model contain significant uncertainty as there are no observations for precipitation and temperature over the ice sheet. For practicality, precipitation values for the '*standard*' run were taken directly from the HadCM3 deglaciation snapshots, but this is the output from only one climate model. Indeed, the current generation of GCMs (Taylor

25   et al., 2012) shows large regional variability in the climatic response to mid-Holocene settings (Harrison et al., 2015), and the GCMs participating in the second phase of the Palaeoclimate Modelling Intercomparison Project (PMIP2 Braconnot et al., 2007) indicated a wet bias for eastern North America (Braconnot et al., 2012). At the time of setting up this study, other climate model output was available and at similar spatial resolution, (e.g. Liu et al. (2009)), but the HadCM3 results are currently the only climate fields produced using the latest boundary conditions for the period, including the ICE-6G_c reconstruction that

30   we initialised our ice sheet from. In fact, HadCM3 has been shown to perform well at simulating the period (see discussion within Morris et al., 2018, Supporting Information), yet even with the latest protocol, there is uncertainty in the model boundary conditions used to run the climate simulations (e.g. see Ivanovic et al., 2016). Ice sheet topography in the GCM simulations (ICE-6G_c) is likely to be a particular source of error, with precipitation being negatively correlated with elevation (Bonacina et al., 1945). For context, the LIS in ICE-6G_c and GLAC-1D reconstructions have distinctly different topographies at 10 ka

(fig. 5), with the three domes and the ice saddle being considerably lower in ICE-6G_c. However, the choice of using ICE-6G_c in the climate simulations is most consistent with our approach of initialising the ice sheet simulations from ICE-6G_c). A possible source of temporal uncertainty in the precipitation is that, and again for practical purposes, our forcing assumes smooth interpolation between the climate means spaced at 500-year intervals, which is unlikely to accurately represent the

5 detailed evolution of North American climate even if it does capture the large-scale glacial-interglacial trends. Nevertheless, it is interesting to see how the ice sheet model responds to the gradual nature of the forcing and more detailed temporal precipitation fields from climate models using the latest and most physically robust boundary conditions are not yet available.

Any biases in the input precipitation can affect the surface mass balance, for example through anomalous accumulation of snow that transforms to ice, and the smaller PDD factor of snow compared to that of ice resulting in excessive snow cover

10 slowing down surface melt. Thus, it is valuable to gain a more rigorous understanding of the impact of the input precipitation fields on our simulated ice sheet evolution. Fig. 9 shows the evolution of the ice sheet thickness in three simulations with different precipitation fields $P(t,x,y)$. For 'precip_0.75' the P field in 'standard' is multiplied by 0.75 (25% reduction), and for 'precip_half' the P field is halved while other model parameters are kept constant.
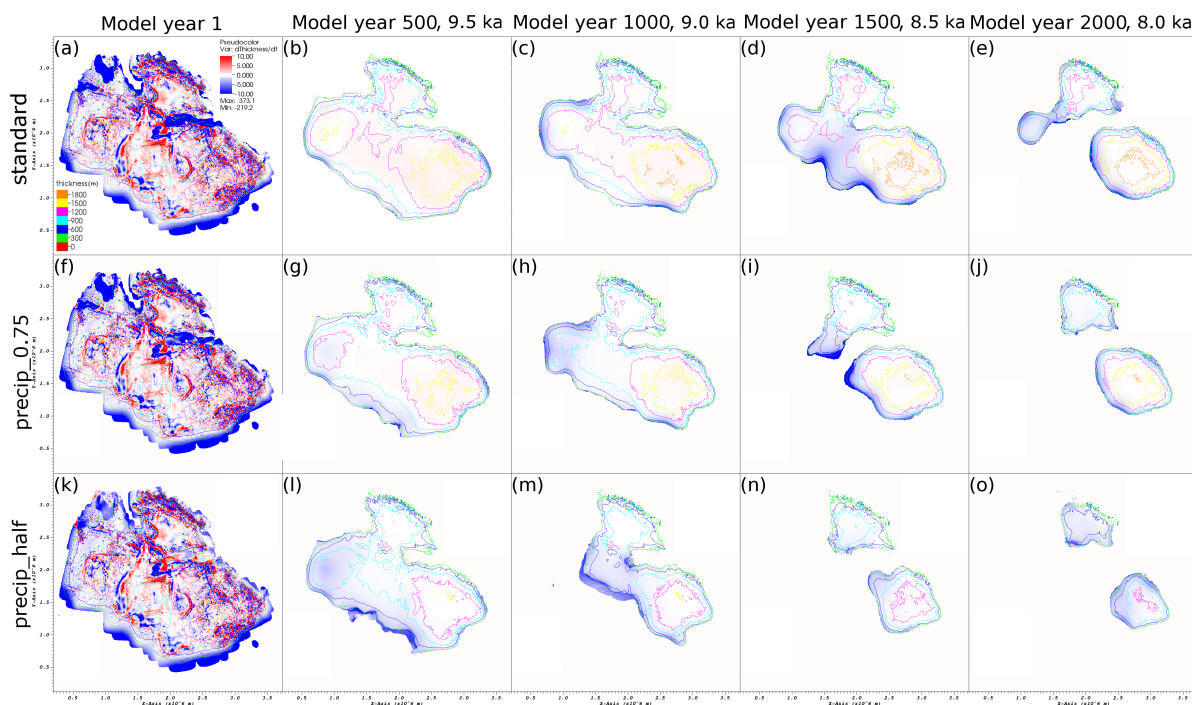

Figure 9. Ice sheet thickness evolution in the three simulations with varying precipitation fields in 500 -year intervals. **(a)**–**(e)** 'standard', **(f)**–**(j)** 'precip_0.75' (P field in 'standard' multiplied by 0.75), and **(k)**–**(o)** 'precip_half'(P field in 'standard' halved)

.

Scaling the input precipitation while keeping the temperature constant can be considered unphysical because the two fields

15 are cliamatologically interdependent, with precipitation usually increasing with temperature (Trenberth and Shea, 2005; Harri-

22

son et al., 2015). However, it is useful to separate out the role of the two fields since they are not linearly related, and hence one of the objectives of this study is to assess the sensitivity of the model setup to individual parameters. Separating temperature from precipitation in this idealised way allows for better understanding of the impact that the precipitation boundary condition has on simulated ice sheet evolution.

5 As described in the previous subsections, the accumulation of ice results in the growth of the Foxe and Labrador domes over the majority of the simulations. Decreasing the input precipitation results in faster deglaciation of the southwestern parts of the ice sheet, namely the Keewatin dome and the modern southern Hudson Bay region.

The importance of the precipitation field is highlighted by the time series describing the volumetric changes of LIS over time (fig. 6e). The modelled separation of the Keewatin and Labrador domes and peak freshwater fluxes in simulations with smaller

10 P occur approximately 400 and 700 years earlier than in 'standard' for 'precip_0.75' and 'precip_half' respectively. The rate of change in the total volume of the ice sheet also changes significantly as a result of decreasing the precipitation (dashed lines in fig. 6e), as already by model year 1000 approximately 65% (42%) of the total initial volume of ice has deglaciated in 'precip_half' ('precip_0.75'), as opposed to approximately 15% of volumetric loss in 'standard'. Thus, LIS is extremely sensitive to variations in the precipitation field and the resulting changes in surface mass balance.

15 **6 Discussion**

The simulated early-Holocene deglaciation of the LIS in 'standard' is in agreement with the sequence of parts of the ice sheet becoming ice-free and their timing is mainly within the reported error estimate of ~500–800 years with the ice extent reconstruction of the North American Ice Sheet (Dyke, 2004, fig. 5). The rate of overall LIS ice loss differs from the GLAC-1D and ICE-6G_c reconstructions for the 10–9 ka period (fig. 4), but the simulated decrease in ice volume over the 9–8 ka period is

20 close to the GLAC-1D reconstruction. The area covered by 8 ka, is within 20% of the reconstructions with extents of $2.36 \cdot 10^6$ km^2, $2.25 \cdot 10^6$ km^2 and $2.01 \cdot 10^6$ km^2 respectively for ICE-6G_c, GLAC-1D and the 'standard' simulation. The ice is thickest at 8 ka in 'standard', with the majority of the difference arising from the simulated Labrador Dome ice volume (1.99 m, 2.63 m and 4.50 m of sea level rise equivalent respectively in ICE-6G_c, GLAC-1D and 'standard'). The Labrador Dome ice volume at ~8.2 ka has recently been estimated at 3.6 ± 0.4 m of eustatic SLR after (Ullman et al., 2016).

25 The 3.8 m ka^{-1} volumetric change over the 10–8 ka period in the 'standard' simulation is smaller than the eustatic SLR for 11.4–8.2 ka based on sea level records (~15 m ka^{-1}; Lambeck et al., 2014). The majority of the SLR in the early Holocene has been attributed to the LIS, with Antarctic contribution estimated at 0.25–0.3 m ka^{-1} (Briggs and Tarasov, 2013). The simulated ice loss over the modelled period is also smaller than the estimated volumetric change in GLAC-1D & ICE-6G_c reconstructions (~5 m ka^{-1} LIS contribution over 10–8 ka). The simulated ice volume in SLR equivalent at 8 ka is however

30 nearer the estimated Labrador Dome volume at ~8.2 ka (Ullman et al., 2016) than the ICE-6G_c estimate. This, together with the higher ice volume in GLAC-1D through 10–8 ka suggests that the initial ice volume in the simulations could be underestimated.

A major feature that differs in the pattern of deglaciation between the ICE-6G_c and 'standard' is the thickening of the three ice domes and the ice saddle over 10–9 ka in the simulation, which results in a comparable ice volume by 9 ka (8.89 m SLR equivalent) with GLAC-1D (9.24 m SLR equivalent), both significantly higher than the ICE-6G_c estimate (4.84 m SLR equivalent). Another pattern that is not present in 'standard' is the opening of the Tyrell Sea at ~9 ka in ICE-6G_c (figures

5   5c and 5h). Instead of the unrealistic opening of a hole in the middle of the ice sheet (which is how the Tyrell Sea opens in ICE-6G_c), BISICLES simulates accumulation and ice flow from the surrounding regions, resulting in thickening of the part of the ice sheet covering the Hudson Bay. At 8 ka, i.e. after the model has integrated for 2000 years (fig. 5j), the simulated ice sheet is more similar to the GLAC-1D reconstruction (fig. 5o) than the ICE-6G_c reconstruction (fig. 5e). This similarity likely results from both the GLAC-1D reconstruction and these BISICLES simulations being based on dynamical ice sheet

10 modelling and driven by a climate forcing, suggesting that having a dynamical component with a climate forcing is important for accurately reconstructing and modelling the LIS in order for the shape of the ice sheet to be physically consistent with ice dynamics.

The opening of the Hudson Bay by an ice saddle collapse is a feature of particular interest due to its potential role as a major forcing for the 8.2 ka event (Matero et al., 2017), and understanding the dynamical changes and resulting freshwater

15 flux motivated setting up this experiment. The modelled opening in 'standard' occurs at model year 1736, which corresponds to 8.26 ka, close to the timing in GLAC-1D (8.2–8.1 ka) and coeval with ICE-6G_c (between 8.5–8.0 ka; fig. 5d). These dates are based on the opening of a completely ice-free corridor between the two domes. Exchange of water masses between the Tyrell Sea and Lake Agassiz likely commenced earlier, as soon as the ice saddle thinned sufficiently to reach flotation (~500 m, assuming the modelled Hudson Bay basal topography and that water level was at sea level on both sides of the ice saddle).

20 The model setup is most sensitive to perturbations related to the surface mass balance (Table 2), which highlights the importance of carefully defining the atmospheric boundary conditions. Higher basal traction coefficients generally result in slower deglaciation (section 5.3) due to less transport of ice towards lower altitudes where melting is more pronounced because of the temperature-elevation feedback, as well as less dynamical ice loss at the marine and lacustrine margins. Higher PDD factors (section 5.4) or alternatively less accumulation through lower precipitation (section 5.6) result in a more negative surface

25 mass balance. Out of the studied parameters, the most significant differences in terms of rate of volumetric loss thus arose from the PDD factors and varying the amount of precipitation.

Note that the importance of each parameter cannot be directly compared in a quantifiable way, as the ranges used for the sensitivity analysis represent something different for each parameter, and were choices based on previous studies. For example, changing the precipitation affects the whole domain, whereas varying the sub-shelf melt rate only affects the floating part of

30 the ice sheet. The sensitivity to different parameters is therefore unlikely to vary in a similar way as a response to halving or doubling a specific model parameter, but their relative importance and interactions between the parameters can be examined.

As a result of the SMB having such an important role in the simulations (see sections 5.4 and 5.6), under- or overestimating the precipitation or values for PDD-factors can have a big impact on the modelled behaviour of the ice sheet. Accurately representing the climate in general circulation models for time periods different from the present is challenging, and different

35 GCMs project regionally heterogeneous patterns of precipitation and temperature for both the future (Knutti et al., 2010) and

Table 2. Peak FWF duration, amplitude and timing (model years since the start of the simulation) in each simulation. The peak is defined as ongoing when the amplitude is greater than the background flux of 0.05 Sv (as defined in section 5.1). The 'n/a' for simulations 'btrc_6x' & 'low_PDD' indicates the peak and the saddle collapse not occurring prior to the end of analysed period of 2000 model years.

Parameter	Duration	Amplitude	Timing	Reference
'standard'	690	0.11	1724	5.1
'AMR_0'	726	0.11	1729	5.2
'AMR_2'	690	0.11	1704	5.2
'btrc_4x'	334	0.07	1798	5.3
'btrc_6x'	n/a	n/a	n/a	5.3
'low_PDD'	n/a	n/a	n/a	5.4
'high_PDD'	301	0.07	1480	5.4
'low_ss_melt'	>705	0.11	1824	5.5
'high_ss_melt'	693	0.13	1697	5.5
'precip_075'	408	0.08	1418	5.6
'precip_half'	1198	0.09	778	5.6

different time periods during the last deglaciation (e.g. Braconnot et al., 2012). For the mid-Holocene, the ensemble averages of GCMs participating in the second phase of the Palaeoclimate Modelling Intercomparison Project (PMIP2; Braconnot et al., 2012) indicated a wet bias for eastern North America compared to reconstructions (fig. 1 in Braconnot et al., 2012). While the fact that the models indicate wetter than reconstructed conditions east of Hudson Bay for the mid-Holocene does not imply

5   that the same is true for the early Holocene, they do suggest that the model representation of precipitation from a single GCM includes significant uncertainty in the region. If the modelled precipitation rates are too high, this could have a knock-on effect resulting in other model parameters such as basal traction and the PDD factors having been tuned to compensate for an unrealistically high accumulation rate.

The large proglacial Lake Agassiz and its interactions with the ice sheet and the climate are another source of uncertainty

10   for modelling the LIS deglaciation. The area and surface temperatures of the lake are poorly constrained, and refining its representation in the climate forcing would affect the availability of moisture for precipitation. Additionally, the lake level is set to sea level in our model setup, whereas the lake could have been up to 770 *m* above sea level prior to its final drawdown (Teller et al., 2002). The elevated water body could have accelerated the ice melt at the southwest margin of the ice sheet due to increased flotation subjecting a larger area of the ice sheet to sub-shelf melting. The model does not, however, distinguish

15   between freshwater and marine margins, and freshwater calving is typically about an order of magnitude lower than for marine margins in comparable settings (Benn et al., 2007b, and references therein). Finally, Lake Agassiz potentially acted as a source

of heat at the ice-water interface, as the bed of Lake Agassiz was sloped towards the ice sheet and the density maximum of freshwater is above the freezing point (as opposed to seawater). Significant absorption of shortwave radiation to the lake could thus have resulted in transport of heat towards the base of the ice sheet through a flow of the warmest and densest water masses, and could have acted as an additional driver of retreat of the lacustrine ice front.

5 ## 7   Conclusions

This is the first application of the BISICLES ice sheet model (Cornford et al., 2013) in the new palaeo setting of North American Ice Sheet deglaciation, and is an effort combining data from multiple sources. The input datasets have their inherent uncertainties, as does the geological evidence used for evaluating the performance of the model setup. As a result of the sensitivity study, a model setup with ranges for key model parameters for early-Holocene LIS deglaciation experiments is

10 established. The importance of accurately representing the LIS ice dynamics during the 10–8 ka period is highlighted by the ice flow in the simulations being highly sensitive to tuning the basal traction coefficient, and the alternate representations of this parameter in the simulations result in the timing of the opening of the Hudson Bay differing by 50–250 years. Accurately representing the model parameters influencing the surface mass balance of the ice sheet (PDD factors and ice topography) and input climatologies (surface air temperature and precipitation) is challenging due to lack of constraining data, but crucial for

15 the model setup due to the deglaciation being largely driven by negative surface mass balance (e.g. Carlson et al., 2009).

The agreement of the pattern of deglaciation between simulations and the reconstructed extent (Dyke, 2004) suggests that the model setup can be a useful tool for evaluating the evolution of the early-Holocene Laurentide Ice Sheet with unprecedented model resolution and representation of the ice dynamics. Recent ice sheet reconstructions (Tarasov et al., 2012; Peltier et al., 2015) provide possible deglacial histories for the demise of the Laurentide Ice Sheet, but not in sufficient detail to evaluate the

20 meltwater flux resulting from a particular feature of interest, the ice saddle collapse over Hudson Bay (Gregoire et al., 2012). The meltwater pulse from this saddle collapse has been hypothesised as having been the primary forcing of the 8.2 ka cooling event (Matero et al., 2017), and these initial simulations reproduce the collapse with a realistic timing between 8.5–8.0 ka (Dyke, 2004; Ullman et al., 2016).

Geoscientific
Model Development
Discussions

References

Abe-Ouchi, A., Segawa, T., and Saito, F.: Climatic conditions for modelling the Northern Hemisphere ice sheets throughout the ice age cycle, Climate of the Past, 3, 423–438, 2007.

Amante, C. and Eakins, B. W.: ETOPO1 1 arc-minute Global Relief Model: Procedures, Data Sources and Analysis, NOAA Technical
5   Memorandum NESDIS, NGDC-24, 2009.

Bassis, J. N., Petersen, S. V., and Mac Cathles, L.: Heinrich events triggered by ocean forcing and modulated by isostatic adjustment, Nature, 542, 332, 2017.

Bauer, E. and Ganopolski, A.: Comparison of surface mass balance of ice sheets simulated by positive-degree-day method and energy balance approach, Climate of the Past, 13, 819, 2017.

10   Benn, D. I., Hulton, N. R., and Mottram, R. H.: Calving laws, sliding laws and the stability of tidewater glaciers, Annals of glaciology, 46, 123–130, 2007a.

Benn, D. I., Warren, C. R., and Mottram, R. H.: Calving processes and the dynamics of calving glaciers, Earth-Science Reviews, 82, 143–179, 2007b.

Blackwell, D. D. and Steele, J. L.: Geothermal Map of North America, Geological Society of America, 1992.

15   Bonacina, L., Poulter, R., Ashmore, S., and Manley, G.: Orographic rainfall and its place in the hydrology of the globe, Quarterly Journal of the Royal Meteorological Society, 71, 41–55, 1945.

Braconnot, P., Otto-Bliesner, B., Harrison, S., Joussaume, S., Peterchmitt, J.-Y., Abe-Ouchi, A., Crucifix, M., Driesschaert, E., Fichefet, T., Hewitt, C., et al.: Results of PMIP2 coupled simulations of the Mid-Holocene and Last Glacial Maximum–Part 1: experiments and large-scale features, Climate of the Past, 3, 261–277, 2007.

20   Braconnot, P., Harrison, S. P., Kageyama, M., Bartlein, P. J., Masson-Delmotte, V., Abe-Ouchi, A., Otto-Bliesner, B., and Zhao, Y.: Evaluation of climate models using palaeoclimatic data, Nature Climate Change, 2, 417, 2012.

Briggs, R. D. and Tarasov, L.: How to evaluate model-derived deglaciation chronologies: a case study using Antarctica, Quaternary Science Reviews, 63, 109–127, 2013.

Carlson, A., Anslow, F., Obbink, E., LeGrande, A., Ullman, D., and Licciardi, J.: Surface-melt driven Laurentide Ice Sheet retreat during the
25   early Holocene, Geophysical Research Letters, 36, 2009.

Charbit, S., Dumas, C., Kageyama, M., Roche, D., and Ritz, C.: Influence of ablation-related processes in the build-up of simulated Northern Hemisphere ice sheets during the last glacial cycle, The Cryosphere, 7, 681, 2013.

Clarke, G. K.: Subglacial processes, Annu. Rev. Earth Planet. Sci., 33, 247–276, 2005.

Clarke, G. K. C., Leverington, D. W., Teller, J. T., and Dyke, A. S.: Paleohydraulics of the last outburst flood from glacial Lake Agassiz
30   and the 8200 BP cold event, Quaternary Science Reviews, 23, 389–407, https://doi.org/10.1016/j.quascirev.2003.06.004, http://www.sciencedirect.com/science/article/pii/S0277379103002865, 2004.

Cornford, S. L., Martin, D. F., Graves, D. T., Ranken, D. F., Le Brocq, A. M., Gladstone, R. M., Payne, A. J., Ng, E. G., and Lipscomb, W. H.: Adaptive mesh, finite volume modeling of marine ice sheets, Journal of Computational Physics, 232, 529–549, https://doi.org/10.1016/j.jcp.2012.08.037, http://www.sciencedirect.com/science/article/pii/S0021999112005050, 2013.

35   Cornford, S. L., Martin, D. F., Payne, A. J., Ng, E. G., Le Brocq, A. M., Gladstone, R. M., Edwards, T. L., Shannon, S. R., Agosta, C., van den Broeke, M. R., Hellmer, H. H., Krinner, G., Ligtenberg, S. R. M., Timmermann, R., and Vaughan, D. G.: Century-scale simulations of the

response of the West Antarctic Ice Sheet to a warming climate, The Cryosphere, 9, 1579–1600, https://doi.org/10.5194/tc-9-1579-2015, https://www.the-cryosphere.net/9/1579/2015/, 2015.

Cornford, S. L., Martin, D. F., Lee, V., Payne, A. J., and Ng, E. G.: Adaptive mesh refinement versus subgrid friction interpolation in simulations of Antarctic ice dynamics, Annals of Glaciology, pp. 1–9, https://doi.org/10.1017/aog.2016.13, https://www.cambridge.org/core/journals/annals-of-glaciology/article/adaptive-mesh-refinement-versus-subgrid-friction-interpolation-in-simulations-of-antarctic-ice-dynamics/E4C4E3039F1A310AF74EBF9C77A2447E, 2016.

Dupont, T. and Alley, R.: Assessment of the importance of ice-shelf buttressing to ice-sheet flow, Geophysical Research Letters, 32, 2005.

Durand, G., Gagliardini, O., Zwinger, T., Le Meur, E., and Hindmarsh, R. C.: Full Stokes modeling of marine ice sheets: influence of the grid size, Annals of Glaciology, 50, 109–114, 2009.

Dyke, A. S.: An outline of North American deglaciation with emphasis on central and northern Canada, Dev. Quat. Sci., 2, 373–424, 2004.

Favier, L., Durand, G., Cornford, S. L., Gudmundsson, G. H., Gagliardini, O., Gillet-Chaulet, F., Zwinger, T., Payne, A. J., and Le Brocq, A. M.: Retreat of Pine Island Glacier controlled by marine ice-sheet instability, Nature Clim. Change, 4, 117–121, https://doi.org/10.1038/nclimate2094, http://www.nature.com/nclimate/journal/v4/n2/full/nclimate2094.html?foxtrotcallback=true, 2014.

Gandy, N., Gregoire, L. J., Ely, J. C., Clark, C. D., Hodgson, D. M., Lee, V., Bradwell, T., and Ivanovic, R. F.: Marine ice sheet instability and ice shelf buttressing of the Minch Ice Stream, northwest Scotland, The Cryosphere, 12, 3635–3651, 2018.

Gladstone, R., Schafer, M., Zwinger, T., Gong, Y., Strozzi, T., Mottram, R., Boberg, F., and Moore, J. C.: Importance of basal processes in simulations of a surging Svalbard outlet glacier, The Cryosphere, 8, 1393–1405, 2014.

Goelzer, H., Robinson, A., Seroussi, H., and Van De Wal, R. S.: Recent Progress in Greenland Ice Sheet Modelling, Current Climate Change Reports, 3, 291–302, 2017.

Gregoire, L. J., Payne, A. J., and Valdes, P. J.: Deglacial rapid sea level rises caused by ice-sheet saddle collapses, Nature, 487, 219–222, https://doi.org/10.1038/nature11257, http://www.nature.com/nature/journal/v487/n7406/abs/nature11257.html, 2012.

Gregoire, L. J., Valdes, P. J., and Payne, A. J.: The relative contribution of orbital forcing and greenhouse gases to the North American deglaciation, Geophysical Research Letters, 42, 9970–9979, 2015.

Gregoire, L. J., Otto-Bliesner, B., Valdes, P. J., and Ivanovic, R.: Abrupt Bølling warming and ice saddle collapse contributions to the Meltwater Pulse 1a rapid sea level rise, Geophysical research letters, 43, 9130–9137, 2016.

Gregoire, L. J., Ivanovic, R. F., Maycock, A. C., Valdes, P. J., and Stevenson, S.: Holocene lowering of the Laurentide ice sheet affects North Atlantic gyre circulation and climate, Climate Dynamics, pp. 1–17, 2018.

Harrison, S. P., Bartlein, P., Izumi, K., Li, G., Annan, J., Hargreaves, J., Braconnot, P., and Kageyama, M.: Evaluation of CMIP5 palaeo-simulations to improve climate projections, Nature Climate Change, 5, 735, 2015.

Hooke, R.: Flow law for polycrystalline ice in glaciers: Comparison of theoretical predictions, laboratory data, and field measurements, Rev. Geophys., 19, 664–672, https://doi.org/10.1029/RG019i004p00664, http://onlinelibrary.wiley.com/doi/10.1029/RG019i004p00664/abstract, 1981.

Ivanovic, R. F., Gregoire, L. J., Roche, D. M., Valdes, P. J., and Peltier, W. R.: Transient climate simulations of the deglaciation 21-9 thousand years before present (version 1)-PMIP4 Core experiment design and boundary conditions, Geoscientific Model Development, 9, 2563, 2016.

Iverson, N. R.: Shear resistance and continuity of subglacial till: hydrology rules, Journal of Glaciology, 56, 1104–1114, 2010.

Geoscientific
Model Development
Discussions

Kaufman, D. S., Ager, T. A., Anderson, N. J., Anderson, P. M., Andrews, J. T., Bartlein, P. J., Brubaker, L. B., Coats, L. L., Cwynar, L. C., Duvall, M. L., et al.: Holocene thermal maximum in the western Arctic (0–180 W), Quaternary Science Reviews, 23, 529–560, 2004.

Knutti, R., Furrer, R., Tebaldi, C., Cermak, J., and Meehl, G. A.: Challenges in combining projections from multiple climate models, Journal of Climate, 23, 2739–2758, 2010.

5 Lambeck, K., Rouby, H., Purcell, A., Sun, Y., and Sambridge, M.: Sea level and global ice volumes from the Last Glacial Maximum to the Holocene, PNAS, 111, 15 296–15 303, https://doi.org/10.1073/pnas.1411762111, http://www.pnas.org/content/111/43/15296, 2014.

Lee, V., Cornford, S. L., and Payne, A. J.: Initialization of an ice-sheet model for present-day Greenland, Annals of Glaciology, 56, 129–140, 2015.

Leverington, D. W., Mann, J. D., and Teller, J. T.: Changes in the Bathymetry and Volume of Glacial Lake Agassiz between 9200 and 7700
10 14C yr B.P., Quaternary Research, 57, 244–252, https://doi.org/10.1006/qres.2001.2311, http://www.sciencedirect.com/science/article/pii/S0033589401923117, 2002.

Liu, Z., Otto-Bliesner, B. L., He, F., Brady, E. C., Tomas, R., Clark, P. U., Carlson, A. E., Lynch-Stieglitz, J., Curry, W., Brook, E., Erickson, D., Jacob, R., Kutzbach, J., and Cheng, J.: Transient Simulation of Last Deglaciation with a New Mechanism for Bølling-Allerød Warming, Science, 325, 310–314, https://doi.org/10.1126/science.1171041, http://www.sciencemag.org/content/325/5938/310, 2009.

15 Lochte, A. A., Repschläger, J., Kienast, M., Garbe-Schönberg, D., Andersen, N., Hamann, C., and Schneider, R.: Labrador Sea freshening at 8.5 ka BP caused by Hudson Bay Ice Saddle collapse, Nature Communications, 10, 586, https://doi.org/10.1038/s41467-019-08408-6, https://www.nature.com/articles/s41467-019-08408-6, 2019.

Margold, M., Stokes, C. R., and Clark, C. D.: Reconciling records of ice streaming and ice margin retreat to produce a palaeogeographic reconstruction of the deglaciation of the Laurentide Ice Sheet, Quaternary science reviews, 189, 1–30, 2018.

20 Marshall, S. J., James, T. S., and Clarke, G. K.: North American ice sheet reconstructions at the Last Glacial Maximum, Quaternary Science Reviews, 21, 175–192, 2002.

Martos, Y. M., Catalán, M., Jordan, T. A., Golynsky, A., Golynsky, D., Eagles, G., and Vaughan, D. G.: Heat flux distribution of Antarctica unveiled, Geophysical Research Letters, 44, 2017.

Matero, I., Gregoire, L., Ivanovic, R., Tindall, J., and Haywood, A.: The 8.2 ka cooling event caused by Laurentide ice saddle collapse, Earth
25 and Planetary Science Letters, 473, 205–214, 2017.

Matero, I. S., Gregoire, L. J., and Ivanovic, R. F.: Simulations of the Early Holocene demise of the Laurentide Ice Sheet with BISI-CLES (public trunk r3298) [Data set], UK Polar Data Centre, Natural Environment Research Council, UK Research and Innovation, https://doi.org/10.5285/7E0B2D81-EE71-48D6-A901-3B417D482072, 2019.

Morris, P. J., Swindles, G. T., Valdes, P. J., Ivanovic, R. F., Gregoire, L. J., Smith, M. W., Tarasov, L., Haywood, A. M., and Bacon, K. L.:
30 Global peatland initiation driven by regionally asynchronous warming, Proceedings of the National Academy of Sciences, 115, 4851–4856, 2018.

Motyka, R. J., Hunter, L., Echelmeyer, K. A., and Connor, C.: Submarine melting at the terminus of a temperate tidewater glacier, LeConte Glacier, Alaska, USA, Annals of Glaciology, 36, 57–65, 2003.

Nias, I. J., Cornford, S. L., and Payne, A. J.: Contrasting the modelled sensitivity of the Amundsen Sea Embayment ice streams, Journal
35 of Glaciology, 62, 552–562, https://doi.org/10.1017/jog.2016.40, https://www.cambridge.org/core/journals/journal-of-glaciology/article/contrasting-the-modelled-sensitivity-of-the-amundsen-sea-embayment-ice-streams/77C6EC93AECECEA667CD1CFC7752D582, 2016.

Nick, F., Van der Veen, C. J., Vieli, A., and Benn, D.: A physically based calving model applied to marine outlet glaciers and implications for the glacier dynamics, Journal of Glaciology, 56, 781–794, 2010.

Paterson, W. S. B.: The physics of glaciers, Elsevier, 2016.

Peltier, W. R., Argus, D. F., and Drummond, R.: Space geodesy constrains ice age terminal deglaciation: The global ICE-6G_C (VM5a) model, J. Geophys. Res. Solid Earth, 120, 2014JB011 176, https://doi.org/10.1002/2014JB011176, http://onlinelibrary.wiley.com/doi/10.1002/2014JB011176/abstract, 2015.

Reed, J., Wheeler, J., and Tucholke, B.: Geologic Map of North America - Perspectives and explanation, Decade of North American Geology, pp. 1–28, 2005.

Rignot, E. and Jacobs, S. S.: Rapid bottom melting widespread near Antarctic ice sheet grounding lines, Science, 296, 2020–2023, 2002.

Rignot, E. and Kanagaratnam, P.: Changes in the velocity structure of the Greenland Ice Sheet, Science, 311, 986–990, 2006.

Rignot, E. and Steffen, K.: Channelized bottom melting and stability of floating ice shelves, Geophysical Research Letters, 35, 2008.

Rignot, E., Bamber, J. L., Van Den Broeke, M. R., Davis, C., Li, Y., Van De Berg, W. J., and Van Meijgaard, E.: Recent Antarctic ice mass loss from radar interferometry and regional climate modelling, Nature geoscience, 1, 106, 2008.

Rignot, E., Koppes, M., and Velicogna, I.: Rapid submarine melting of the calving faces of West Greenland glaciers, Nature Geoscience, 3, 187, 2010.

Rignot, E., Mouginot, J., and Scheuchl, B.: Ice flow of the Antarctic ice sheet, Science, 333, 1427–1430, 2011.

Rignot, E., Jacobs, S., Mouginot, J., and Scheuchl, B.: Ice-shelf melting around Antarctica, Science, 341, 266–270, 2013.

Rutt, I. C., Hagdorn, M., Hulton, N., and Payne, A.: The Glimmer community ice sheet model, Journal of Geophysical Research: Earth Surface, 114, 2009.

Schoof, C.: Ice sheet grounding line dynamics: Steady states, stability, and hysteresis, Journal of Geophysical Research: Earth Surface, 112, 2007.

Schoof, C. and Hindmarsh, R. C. A.: Thin-Film Flows with Wall Slip: An Asymptotic Analysis of Higher Order Glacier Flow Models, Q J Mechanics Appl Math, 63, 73–114, https://doi.org/10.1093/qjmam/hbp025, https://academic.oup.com/qjmam/article/63/1/73/1843730/Thin-Film-Flows-with-Wall-Slip-An-Asymptotic, 2010.

Shepherd, A. and Wingham, D.: Recent sea-level contributions of the Antarctic and Greenland ice sheets, science, 315, 1529–1532, 2007.

Singarayer, J. S. and Valdes, P. J.: High-latitude climate sensitivity to ice-sheet forcing over the last 120 kyr, Quaternary Science Reviews, 29, 43–55, 2010.

Singarayer, J. S., Valdes, P. J., Friedlingstein, P., Nelson, S., and Beerling, D. J.: Late Holocene methane rise caused by orbitally controlled increase in tropical sources, Nature, 470, 82–85, 2011.

Stokes, C., Margold, M., Clark, C., and Tarasov, L.: Ice stream activity scaled to ice sheet volume during Laurentide Ice Sheet deglaciation., Nature., 530, 322–326, 2016.

Stuhne, G. and Peltier, W.: Assimilating the ICE-6G_C Reconstruction of the Latest Quaternary Ice Age Cycle Into Numerical Simulations of the Laurentide and Fennoscandian Ice Sheets, Journal of Geophysical Research: Earth Surface, 122, 2324–2347, 2017.

Swindles, G. T., Morris, P. J., Whitney, B., Galloway, J. M., Gałka, M., Gallego-Sala, A., Macumber, A. L., Mullan, D., Smith, M. W., Amesbury, M. J., et al.: Ecosystem state shifts during long-term development of an Amazonian peatland, Global change biology, 24, 738–757, 2018.

Tarasov, L. and Peltier, W. R.: A geophysically constrained large ensemble analysis of the deglacial history of the North American ice-sheet complex, Quaternary Science Reviews, 23, 359–388, 2004.

31

Tarasov, L., Dyke, A. S., Neal, R. M., and Peltier, W. R.: A data-calibrated distribution of deglacial chronologies for the North American ice complex from glaciological modeling, Earth and Planetary Science Letters, 315, 30–40, 2012.

Taylor, A. D.: A Model of Iceberg Calving in Greenland, Ph.D. thesis, University of Bristol, 2016.

Taylor, K. E., Stouffer, R. J., and Meehl, G. A.: An overview of CMIP5 and the experiment design, Bulletin of the American Meteorological
5   Society, 93, 485–498, 2012.

Teller, J. T., Leverington, D. W., and Mann, J. D.: Freshwater outbursts to the oceans from glacial Lake Agassiz and their role in climate change during the last deglaciation, Quaternary Science Reviews, 21, 879–887, https://doi.org/10.1016/S0277-3791(01)00145-7, http://www.sciencedirect.com/science/article/pii/S0277379101001457, 2002.

Trenberth, K. E. and Shea, D. J.: Relationships between precipitation and surface temperature, Geophysical Research Letters, 32, 2005.

10   Ullman, D. J., Carlson, A. E., Hostetler, S. W., Clark, P. U., Cuzzone, J., Milne, G. A., Winsor, K., and Caffee, M.: Final Laurentide ice-sheet deglaciation and Holocene climate-sea level change, Quaternary Science Reviews, 152, 49–59, 2016.

Van de Berg, W. J., Van Den Broeke, M., Ettema, J., Van Meijgaard, E., and Kaspar, F.: Significant contribution of insolation to Eemian melting of the Greenland ice sheet, Nature Geoscience, 4, 679, 2011.

Winsborrow, M. C., Clark, C. D., and Stokes, C. R.: What controls the location of ice streams?, Earth-Science Reviews, 103, 45–59, 2010.

15   Zwally, H. J., Abdalati, W., Herring, T., Larson, K., Saba, J., and Steffen, K.: Surface melt-induced acceleration of Greenland ice-sheet flow, Science, 297, 218–222, 2002.